Supporting Information

Inductive and electrostatic effects on cobalt porphyrins for heterogeneous electrocatalytic carbon dioxide reduction

Minghui Zhu[#], Deng-Tao Yang[#], Ruquan Ye, Joy Zeng, Nathan Corbin, and Karthish Manthiram[*]

Department of Chemical Engineering, Massachusetts Institutes of Technology, 77 Massachusetts Ave, Cambridge, MA 02139

E-mail: karthish@mit.edu

[#] These authors contributed equally to this work

1. EXPERIMENTAL METHODS 2

1.1. CHEMICALS 2

1.2. CHEMICAL CHARACTERIZATION 4

1.3. ELECTRODE PREPARATION 10

1.4. MATERIALS CHARACTERIZATION 11

1.5. ELECTROCHEMICAL MEASUREMENT 11

1.6. GC CALIBRATION 13

2. COMPUTATIONAL METHODS 14

3. CALCULATION OF COBALT-COBALT DISTANCE ON CARBON BLACK SUPPORT . . . 17

4. DERIVATION OF THEORETICAL KINETIC PARAMETERS 18

5. ADDITIONAL ELECTROCHEMICAL DATA 19

6. DFT COORDINATES OF OPTIMIZED STRUCTURES 40

7. REFERENCES 45

1. Experimental methods

1.1. Chemicals

Materials. Carbon paper (Toray, TGP-H-060) and carbon black (Vulcan XC 72) were purchased from Fuel Cell Earth. Nafion solution (Nafion-117, 5 wt.%), N,N-dimethylformamide (99.8%), ammonium cobalt(II) sulfate hexahydrate (99%), ammonium hexafluorophosphate (99.99%), hydrochloric acid (ACS reagent, 37%) and sodium carbonate (99.999% trace metal basis) were purchased from Sigma Aldrich. Methanol (≥99.8% ACS), acetone (≥99.5% ACS) and ethyl acetate (≥99.8% ACS) were purchased from VWR. Platinum foil (99.9% metals basis) was purchased from Alfa Aesar. Ag/AgCl reference electrode (LF-2) was purchased from Innovative Instrument Inc. Cobalt tetraphenylporphyrin (CoTPP), cobalt tetramethoxyphenylporphyrin (CoTMPP), cobalt tetrabromophenylporphyrin (CoTBPP), meso-Tetra (N-methyl-2-pyridyl) porphine tetrachloride (H_2TMpyp2), meso-Tetra (N-methyl-3-pyridyl) porphine tetrachloride (H_2TMpyp3), cobalt meso-Tetra (N-methyl-4-pyridyl) porphine tetrachloride (CoTMpyp4) and meso-Tetra(4-N,N,N-trimethylanilinium) porphine tetrachloride (H_2TMAP) were purchased from Frontier Scientific Inc. Cobalt tetrachlorophenylporphyrin (CoTCPP) was purchased from Yuanjiang Hualong Catalyst Technology Co. Ltd. Cobalt tetrasulfonatophenylporphyrin tetrasodium (CoTSPP) was purchased from Atomax Chemicals Co., Ltd. All chemicals were used as received without further purification. CO_2 cylinder (99.999% research grade) was purchased from Airgas.

Synthesis of cobalt tetra-(4-N,N,N-trimethylanilinium)porphyrin. Meso-Tetra(4-N,N,N-trimethylanilinium) porphine tetrachloride (94 mg, 9.5×10^{-5} mol) and ammonium cobalt(II) sulfate hexahydrate (593 mg, 1.5×10^{-3} mol) were added to Milli-Q water (41 mL) and degassed by N_2 for 10 min, after which the solution was stirred at 85° C under N_2 atmosphere for 12 hours. Reaction product is precipitated by adding 10 equivalents NH_4PF_6 (155 mg, 9.5×10^{-4} mol) and centrifuged. The collected solid is further washed with 10 ml Milli-Q water and 10 equivalents NH_4PF_6 (155 mg, 9.5×10^{-4} mol) twice and separated by centrifugation. Afterwards, the residue is dissolved in 9 ml acetone, then 1 ml concentrated HCl (37%) is added dropwise to exchange anilinium counter ions. The mixture is sonicated for 10 min and centrifuged. After the supernatant is removed, the solid phase is collected and washed with 10 ml acetone twice. The residue is then dissolved in 2 ml methanol and precipitated with 1 ml ethyl acetate. The solvent is eventually

removed in vacuum under room temperature to yield CoTMAP powder. The purity of CoTMAP was confirmed by UV-vis, ^{1}H-NMR, and high-resolution mass spectra.

Synthesis of cobalt tetra-(N-methyl-2-pyridyl)porphyrin. Meso-Tetra (N-methyl-2-pyridyl) porphine tetrachloride (78 mg, 9.5×10^{-5} mol) and ammonium cobalt(II) sulfate hexahydrate (593 mg, 1.5×10^{-3} mol) were added to Milli-Q water (41 mL) and degassed by N_2 for 10 min, after which the solution was stirred at 85° C under N_2 atmosphere for 12 hours. Reaction product is precipitated by adding 40 equivalents NH_4PF_6 (620 mg, 3.8×10^{-3} mol) and centrifuged. The collected solid is further washed with 10 ml Milli-Q water and 40 equivalents NH_4PF_6 (620 mg, 3.8×10^{-3} mol) twice and separated by centrifugation. Afterwards, the residue is dissolved in 9 ml acetone, then 1 ml concentrated HCl (37%) is added dropwise to exchange anilinium counter ions. The mixture is sonicated for 10 min and centrifuged. After the supernatant is removed, the solid phase is collected and washed with 10 ml acetone twice. The residue is then dissolved in 2 ml methanol and precipitated with 1 ml ethyl acetate. The solvent is eventually removed in vacuum under room temperature to yield CoTMpyp2 powder. The purity of CoTMpyp2 was confirmed by UV-vis, ^{1}H-NMR, and high-resolution mass spectra.

Synthesis of cobalt tetra-(N-methyl-3-pyridyl)porphyrin. Meso-Tetra (N-methyl-3-pyridyl) porphine tetrachloride (78 mg, 9.5×10^{-5} mol) and ammonium cobalt(II) sulfate hexahydrate (593 mg, 1.5×10^{-3} mol) were added to Milli-Q water (41 mL) and degassed by N_2 for 10 min, after which the solution was stirred at 85° C under N_2 atmosphere for 12 hours. Reaction product is precipitated by adding 40 equivalents NH_4PF_6 (620 mg, 3.8×10^{-3} mol) and centrifuged. The collected solid is further washed with 10 ml Milli-Q water and 40 equivalents NH_4PF_6 (620 mg, 3.8×10^{-3} mol) twice and separated by centrifugation. Afterwards, the residue is dissolved in 9 ml acetone, then 1 ml concentrated HCl (37%) is added dropwise to exchange anilinium counter ions. The mixture is sonicated for 10 min and centrifuged. After the supernatant is removed, the solid phase is collected and washed with 10 ml acetone twice. The residue is then dissolved in 2 ml methanol and precipitated with 1 ml ethyl acetate. The solvent is eventually removed in vacuum under room temperature to yield CoTMpyp3 powder. The purity of CoTMpyp3 was confirmed by UV-vis, ^{1}H-NMR, and high-resolution mass spectra.

1.2. Chemical characterization

High-resolution mass spectra (HRMS) were obtained from an Agilent Technologies 6545 Q-TOF LC/MS spectrometer. ^{1}H-NMR were measured on Bruker AVANCE-400 NMR spectrometer. UV-vis spectra were collected on an Ocean Optics Miniature Spectrometer.

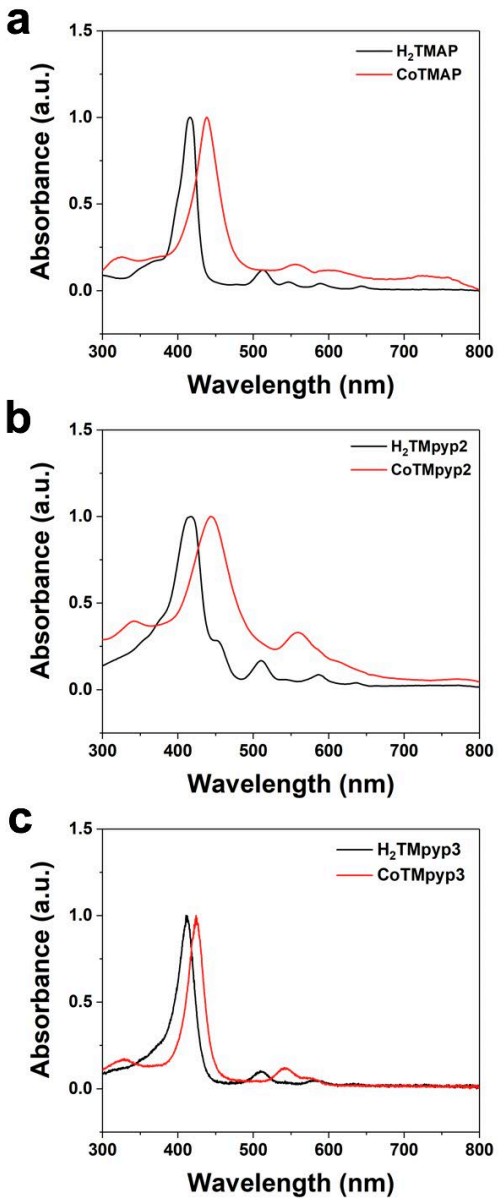

Figure S1. UV-vis spectrum of (a) H_2TMAP and CoTMAP, (b) H_2TMpyp2 and CoTMpyp2, and (c) H_2TMpyp3 and CoTMpyp3 (solvent: H_2O).

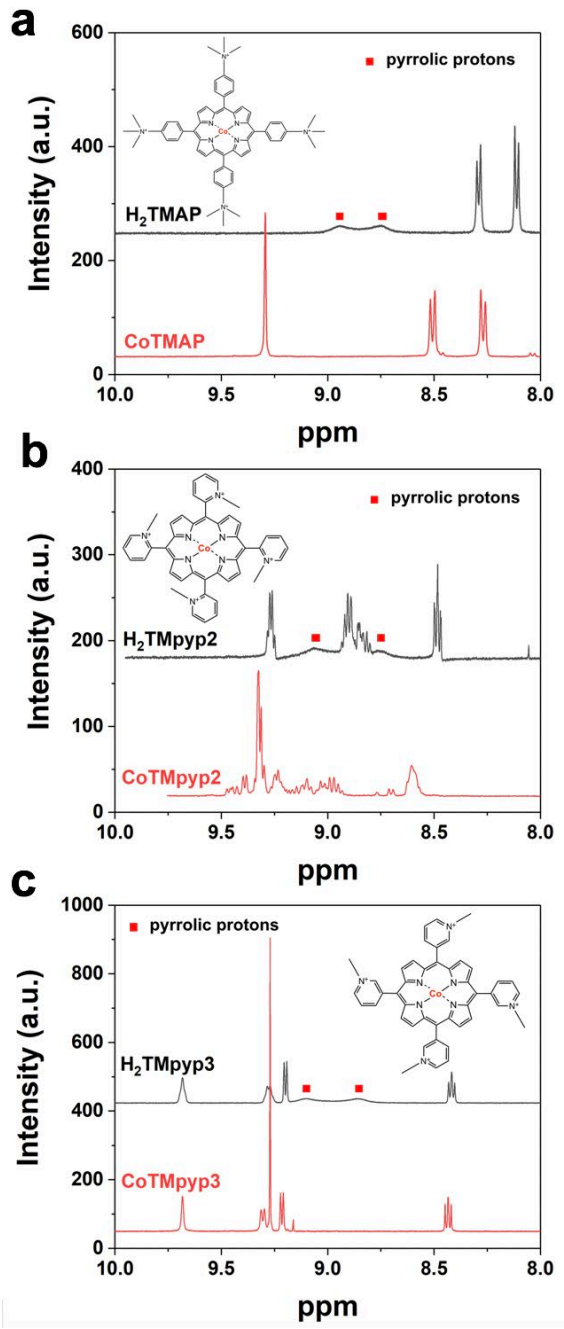

Figure S2. ^{1}H-NMR spectrum of (a) H_2TMAP and CoTMAP, (b) H_2TMpyp2 and CoTMpyp2, and (c) H_2TMpyp3 and CoTMpyp3 (solvent: D_2O).

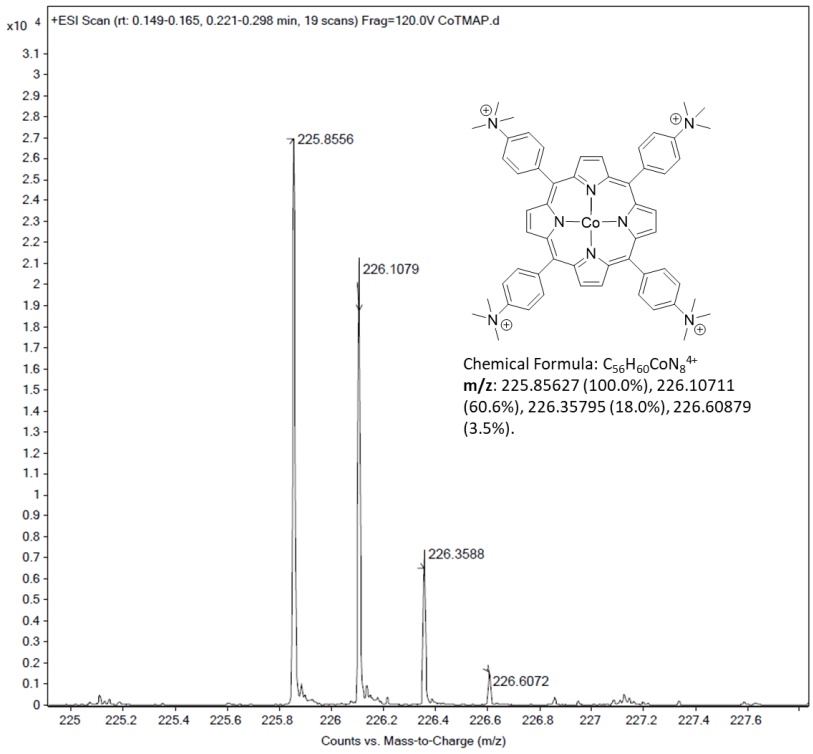

Figure S3. High-resolution mass spectra of CoTMAP.

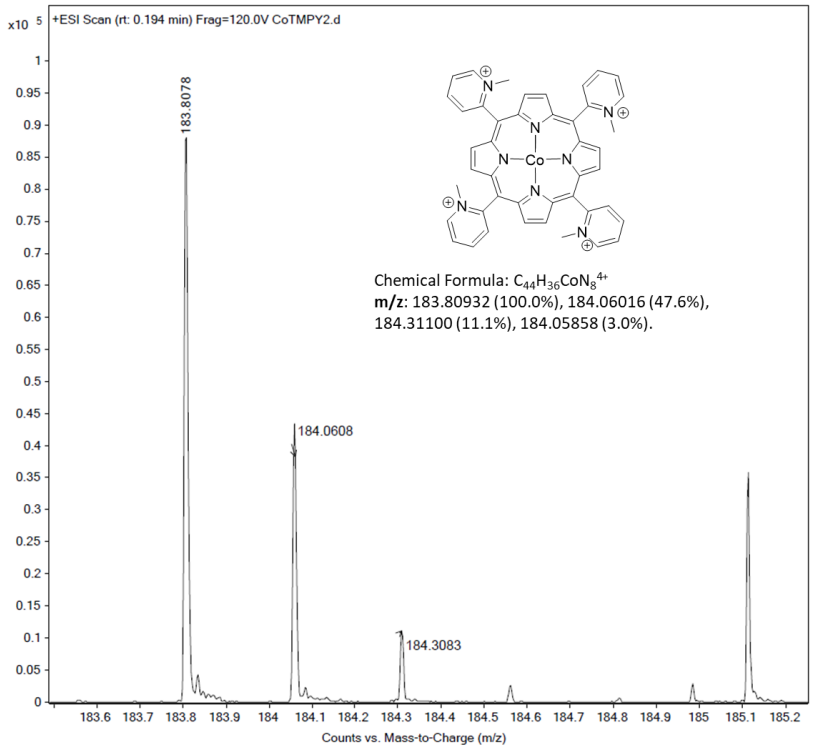

Figure S4. High-resolution mass spectra of CoTMpyp2.

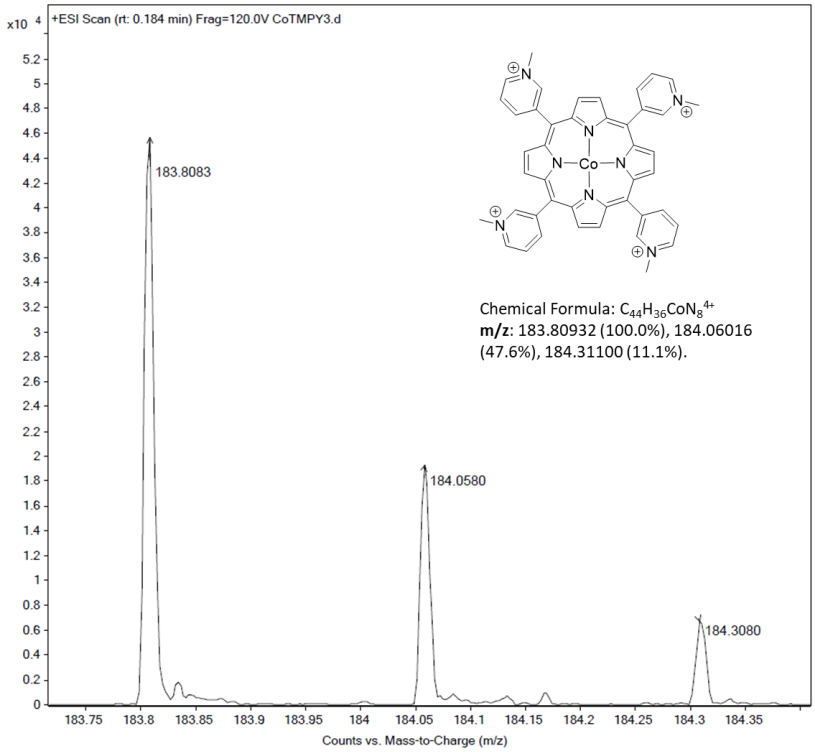

Figure S5. High-resolution mass spectra of CoTMpyp3.

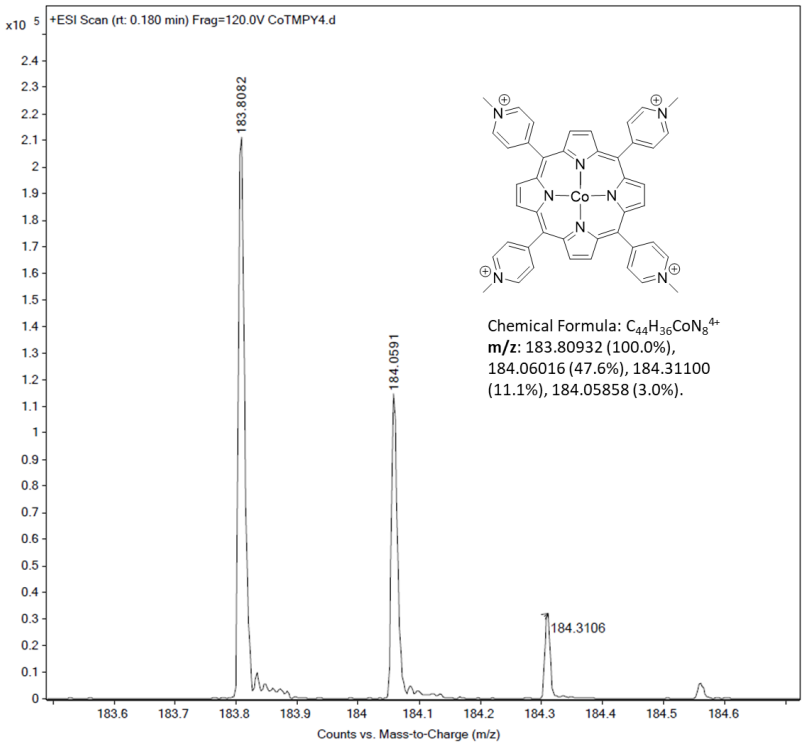

Figure S6. High-resolution mass spectra of CoTMpyp4.

1.3. Electrode preparation

Preparation of hydrophilic carbon paper. Pristine carbon paper was punched to discs with a diameter of 0.5 inch and heated in a tube furnace at 800°C in static air for 10 min before use.

Preparation of working electrode. The porphyrin solution was prepared by adding 17.77 μmol of the desired cobalt porphyrin derivative and 30 μL of Nafion solution into 2 mL N,N-dimethylformamide, followed by 30 minutes of sonication. Carbon black solution was prepared by dispersing 60 mg of carbon black in a mixture of 155 μL of Nafion solution and 20 mL N,N-dimethylformamide with 12 hours of sonication to ensure complete dispersion. The final catalyst ink was then prepared by mixing the porphyrin solution and carbon black solution prepared above at different ratios specified in Table S1 to achieve various porphyrin loadings. The working electrode was then prepared by first drop-casting 15 μL of the prepared catalyst ink on one side of the carbon paper disc, oven-dried in air at 80°C for 30 min, and then drop-casting 15 μL of the ink on the other side of the carbon paper disc, followed by oven-drying in air at 80°C for another 30 min. During dropcasting, the droplet instantaneously spread throughout the entire carbon paper without penetrating onto the underlying aluminum foil.

Table S1. Ink composition for preparing cobalt porphyrin electrodes with various loadings.

Cobalt porphyrin loading (mol/cm^2)	**Volume ratio of porphyrin solution to carbon black solution to produce catalyst ink**
4×10^{-8}	20/80
1×10^{-8}	5/95
4×10^{-9}	2/98
2×10^{-9}	1/99
8×10^{-10}	0.4/99.6
4×10^{-10}	0.2/99.8

1.4. Materials characterization

SEM/EDX was performed on a Zeiss Merlin High-resolution scanning electron microscope with an InLens detector.

1.5. Electrochemical measurement

Cell design. Electrochemical reduction of CO_2 was conducted in a customized three-compartment cell fabricated from polycarbonate, containing a counter electrode compartment, working electrode compartment, and gas compartment. The working electrode compartment was separated from the counter electrode compartment by a Nafion membrane (Figure S7).

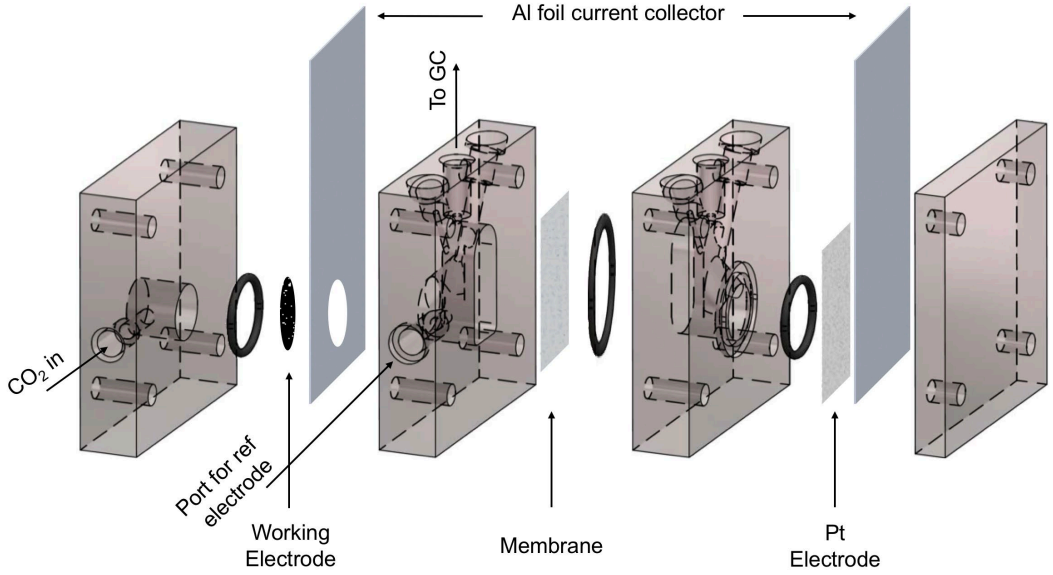

Figure S7. Schematic of the 3-compartment electrochemical cell and setup used in the present study.[1]

Electroreduction of CO_2. The electrochemical measurements were controlled with a VMP3 Multi-channel potentiostat. 0.5 M sodium bicarbonate was prepared by bubbling CO_2 through sodium carbonate solution (0.25 M) overnight. Resistance between the reference electrode and working electrode was determined to be 20 Ω with Potential Electrochemical Impedance Spectroscopy (PEIS) and manually compensated by 85%. Prior to electrochemical measurements, 1.75 mL of electrolyte was added into the working electrode compartment and counter electrode compartment, respectively. 10 sccm of CO_2 gas was purified by an oxygen purifier (Matheson,

MCTG-0051-XX) and controlled by Alicat mass flow controller and introduced into the cell at atmospheric pressure; CO_2 gas enters the cell through the gas compartment, traverses the working electrode, and exits through the working electrode compartment. Cells were purged with CO_2 for 10 min before electrochemical polarization. Gas products were analyzed by an on-line gas chromatograph (SRI Instruments) every 5 min. CO was quantified by an FID detector with methanizer and H_2 was quantified by a TCD detector.

For CO_2 order dependence measurements, CO_2 partial pressure was controlled by changing relative CO_2 and He flow rate to achieve P_{CO2} of 1, 0.8, 0.6, 0.4, 0.2 and 0.1 atm. For bicarbonate order dependence measurements, sodium perchlorate was used as a supporting electrolyte; while sodium bicarbonate concentration was varied from 0.05 M to 0.5 M, proper amount of sodium perchlorate was added to ensure a constant $[Na^+]$ of 0.5 M. pH were measured for each electrolyte composition: 0.05 M $NaHCO_3$ (pH = 6.6), 0.1 M $NaHCO_3$ (pH = 6.9), 0.2 M $NaHCO_3$ (pH = 7.0), 0.3 M $NaHCO_3$ (pH = 7.2) and 0.5 M $NaHCO_3$ (pH = 7.4). Order dependence measurements were performed at constant potential of -1.3 V *vs.* Ag/AgCl.

1.6. GC Calibration

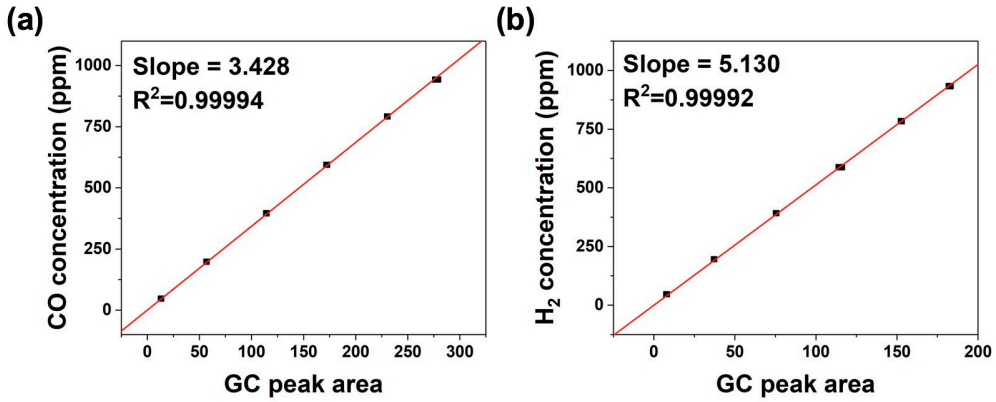

Figure S8. Calibration curve for (a) CO and (b) H_2.

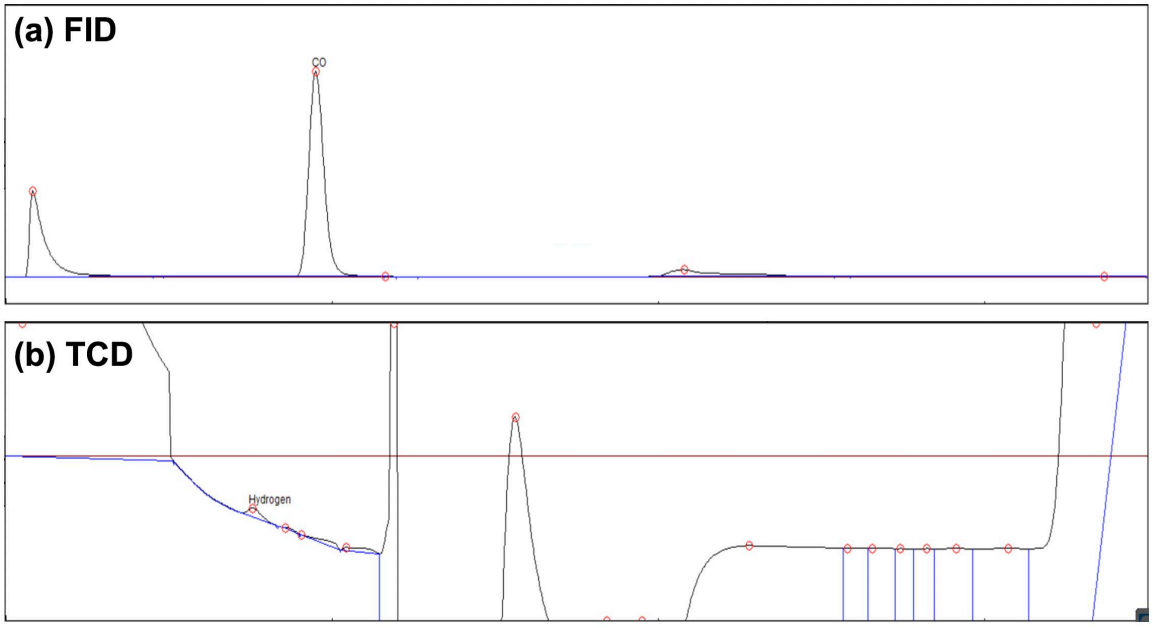

Figure S9. Sample GC signal showing (a) CO signal from FID detector and (b) H_2 signal from TCD detector during a common steady-state electrolysis measurement.

2. Computational methods

The density functional theory (DFT) computations of the inductive effect exerted by substituents were performed at the B3LYP[2–4] level using the standard 6-31g(d)[5,6] basis set implemented in the Gaussian 09 package.[7] The calculated Mulliken charge populations were taken from a probe hydrogen atom attached to the substituent (Figures S10).[8–10] Initial input coordinates were taken from the corresponding structures drawn in GaussView. All the calculated Mulliken charge populations were taken from optimized structures (# opt b3lyp/6-31g(d) geom=connectivity). All coordinates of optimized structures are attached at the end of this Supporting Information (Section 6). Better accuracy for Mulliken charge analysis is typically obtained using a smaller basis set, unlike energy calculations in which a large basis set is more desirable.[11] This is because in Mulliken analysis, half the overlap population is assigned to each contributing orbital, giving the total population of each atomic orbital (OA).[12] It can be problematic if one uses diffuse OAs, where an OA on atom A might actually have a large contribution to adjacent atom B.[13]

Therefore, Mulliken charge populations were computed using basis set 6-31g(d) without diffuse functions. We also tried a triple-z basis set 6-311g(d,p), which provided similar results (Figure S11-13).

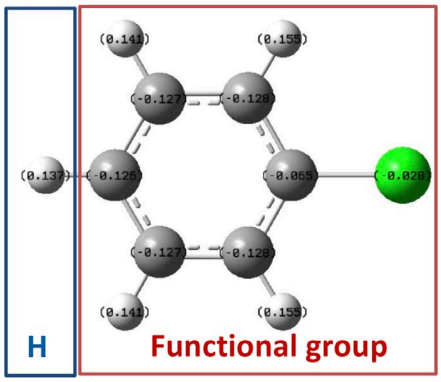

Figure S10. An example showing the electronegativity determination of chlorophenyl (PhCl) in cobalt tetrachlorophenylporphyrin. Structure of H-PhCl and the corresponding Mulliken charge of each atom. The Mulliken charge of the highlighted H atom was used to determine the inductive effect of the -PhCl functional group. (white: H; grey: C; green: Cl)

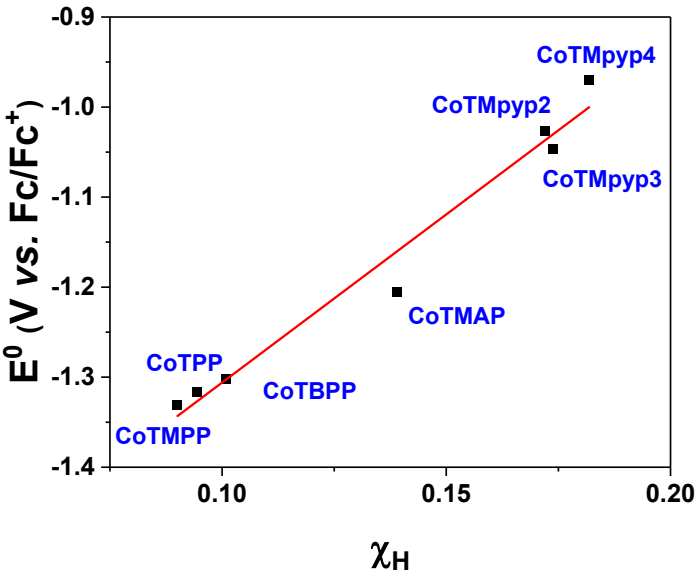

Figure S11. Correlation between calculated χ_H and experimentally measured Co(I/II) redox potentials. (triple-z basis set 6-311g(d,p))

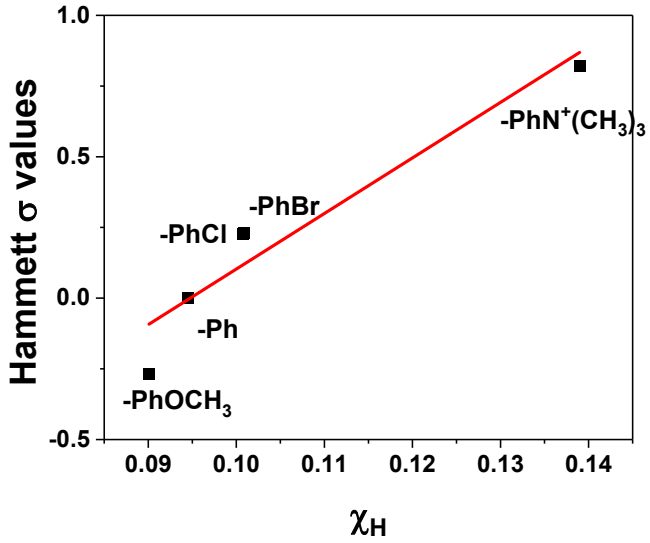

Figure S12. Correlation between calculated χ_H and the corresponding *para* position Hammett substituent constant. (triple-z basis set 6-311g(d,p))

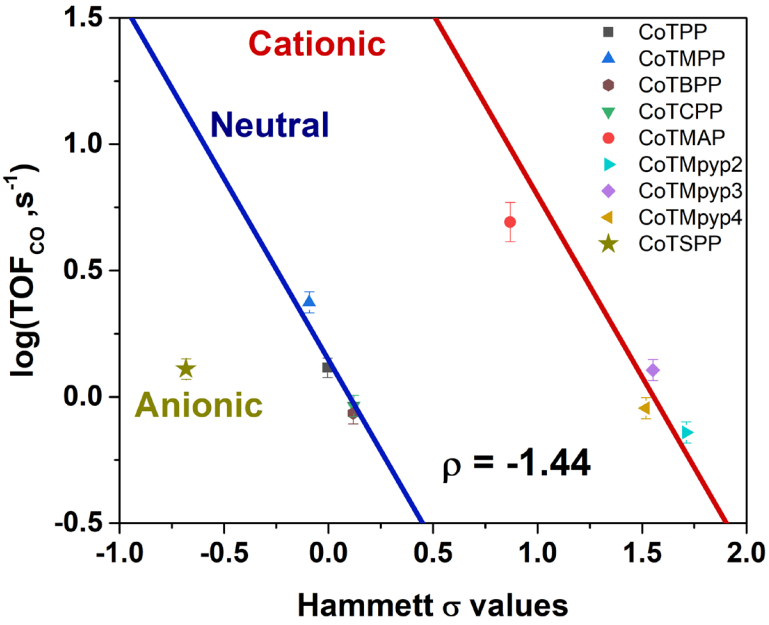

Figure S13. TOF_{CO} of cobalt porphyrin derivatives with various functionalities versus calculated Hammett σ values (potential: -0.6 V *vs.* RHE, loading: 8×10^{-10} mol/cm^2). (triple-z basis set 6-311g(d,p))

3. Calculation of cobalt-cobalt distance on carbon black support

Assuming cobalt porphyrins were evenly distributed on carbon black, we can calculate the theoretical Co-Co distance of two adjacent molecules. At a loading of $2x10^{-9}$ mol/cm^2 where we started to observe maximized TOF_{CO} for CoTPP, the number of CoTPP molecules per gram of carbon black can be calculated based on the electrode composition:

$$\mathrm{N} = \frac{2 \times 10^{-9}\ \ mol/cm^2 \times 6.023 \times 10^{23}\ \ mol^{-1}}{70 \times 10^{-6}\ \ g/cm^2} = 1.72 \times 10^{19}\ \ g^{-1}$$

According to the specification sheet from the manufacturer, Vulcan XC-72 has a surface area of approximately 250 m^2/g. The area per CoTPP molecule can then be derived as:

$$S_{unit\ \ CoTPP} = \frac{250 \times 10^{18}\ \ nm^2/g}{1.72 \times 10^{19}\ \ g^{-1}} = 14.53\ \ nm^2$$

Assuming a square lattice, this corresponds to a Co-Co distance of:

$$Distance_{Co-Co} = \sqrt{14.53}\ \ nm = 3.8\ \ nm$$

4. Derivation of theoretical kinetic parameters

If reduction of reactant CO_2 is limited by an irreversible electron transfer to CO_2, the reaction rate expressed as a partial current for CO is[14]:

$$j_{CO} = nFk\theta P_{CO_2} \exp\left(\frac{\beta F\eta}{RT}\right)$$

where n is the total number of electron transfers needed to convert CO_2 to CO, F is Faraday's constant, k is the rate constant for the rate-determining step, θ is the surface coverage of vacant Co^I active sites, β is the transfer coefficient (assumed to be 0.5), η is the overpotential, R is the gas constant, and T is the temperature. We assume the population of vacant cobalt active sites is approximately equal to the total population of cobalt active sites since the rate determining step involves CO_2 adsorption to a vacant site; this means θ can be considered to be potential independent. In addition, the initial reduction of cobalt ($Co^{II} + e^- \rightarrow Co^I$) is considered to be a fast and irreversible step, such that the population of the vacant Co^I sites θ can be treated as a constant.

The Tafel slope is given by the partial derivative of the overpotential with respect to the logarithm of current, yielding:

$$\left(\frac{\partial\eta}{\partial \log j_{CO}}\right)_{P_{CO_2}} = \frac{2.3RT}{\beta F} = 118 \text{ mV/dec}$$

Such a mechanism has a theoretical Tafel slope of 118 mV/dec, a first order dependence on CO_2, and a zeroth order dependence on bicarbonate[15], consistent with the measured 119 mV/dec Tafel slope, 0.99 order dependence on CO_2, and 0.12 order dependence on bicarbonate.

5. **Additional electrochemical data**

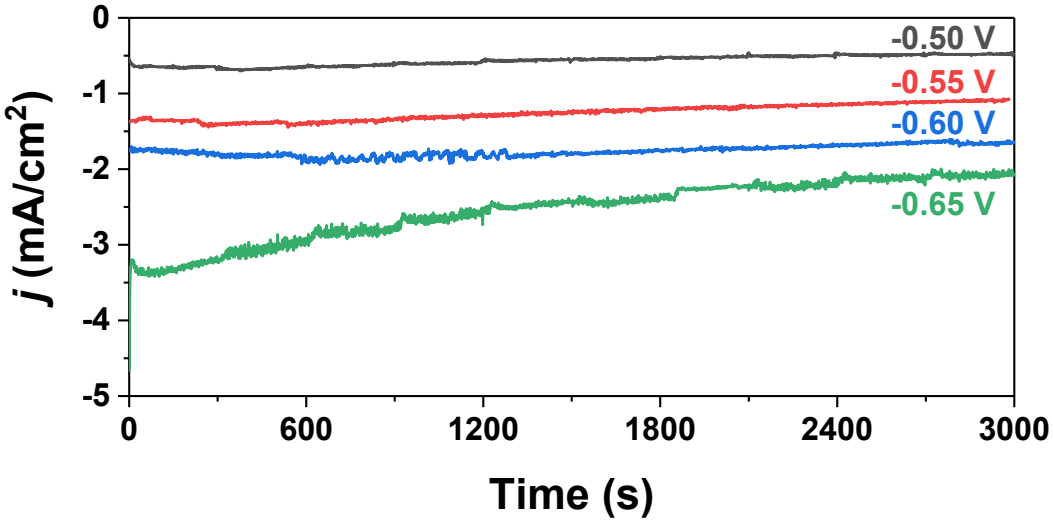

Figure S14. Total current densities of steady-state CO_2 electroreduction catalyzed by CoTPP at different potentials. Electrolyte solution is 0.5 M $NaHCO_3$.

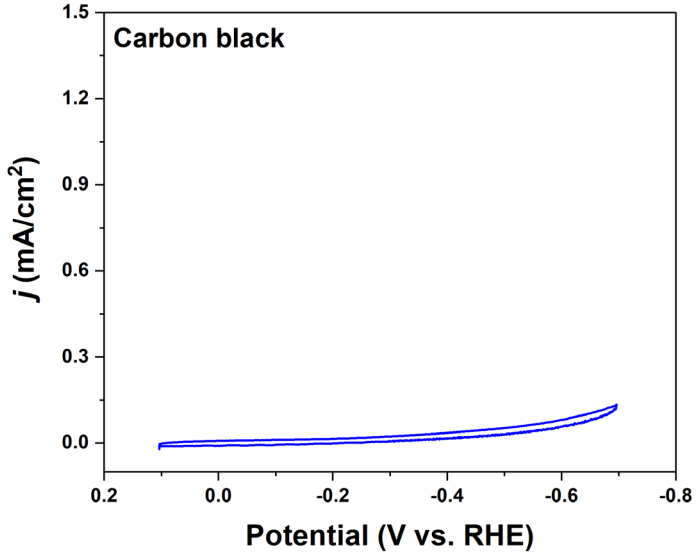

Figure S15. Cyclic voltammograms collected at a sweep rate of 5 mV/s on carbon black (loading: ~70 μg/cm^2) with no cobalt porphyrin catalyst on carbon paper under CO_2. Electrolyte solution is 0.5 M $NaHCO_3$.

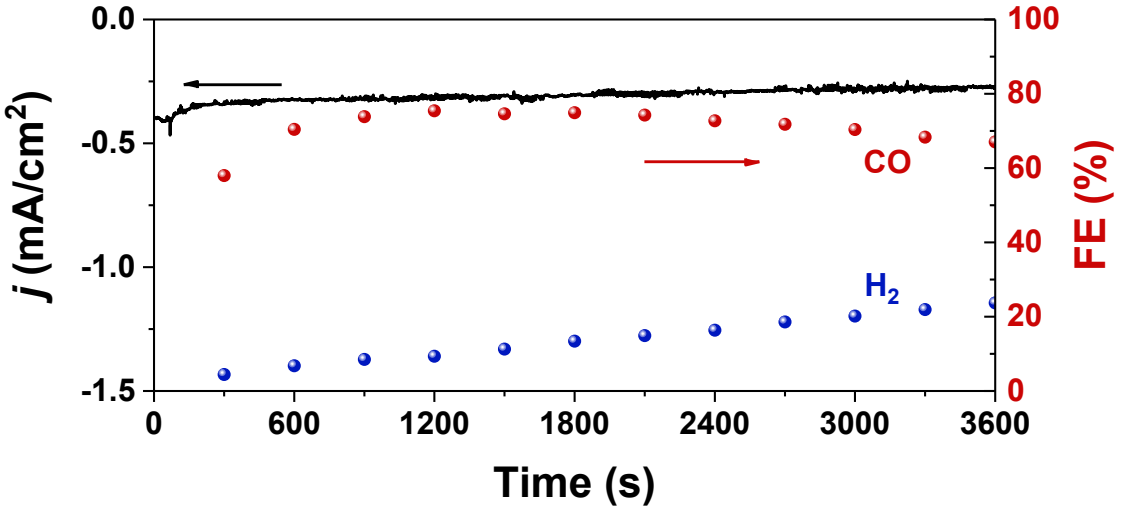

Figure S16. Total current densities and Faradaic efficiencies for CO and H_2 during steady-state CO_2 electroreduction catalyzed by CoTPP (loading: 8×10^{-10} mol/cm^2, potential: -0.6 V *vs.* RHE). Electrolyte solution is 0.5 M $NaHCO_3$.

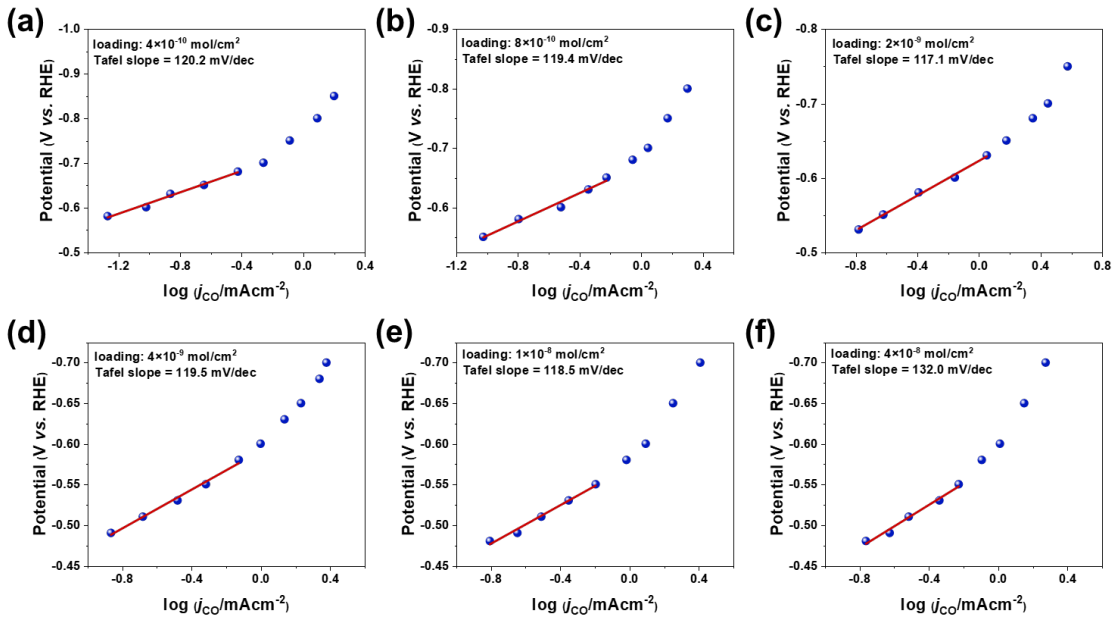

Figure S17. Tafel plot for CoTPP at various loadings. Electrolyte solution is 0.5 M $NaHCO_3$.

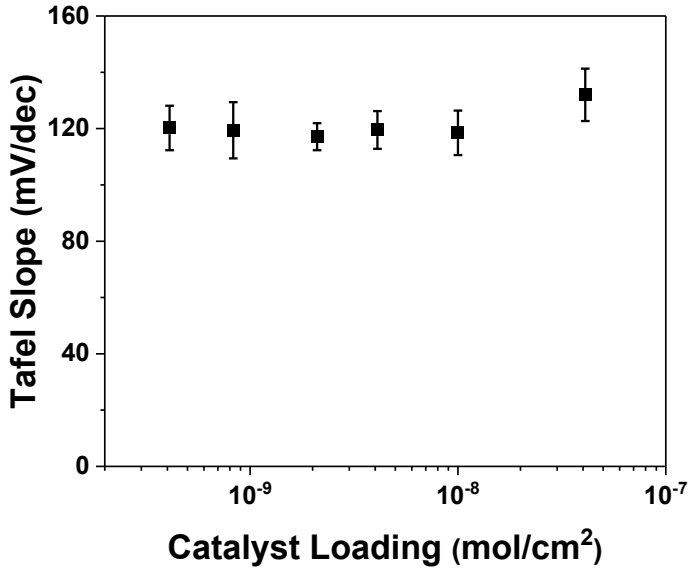

Figure S18. Tafel slopes versus CoTPP loading. Electrolyte solution is 0.5 M $NaHCO_3$.

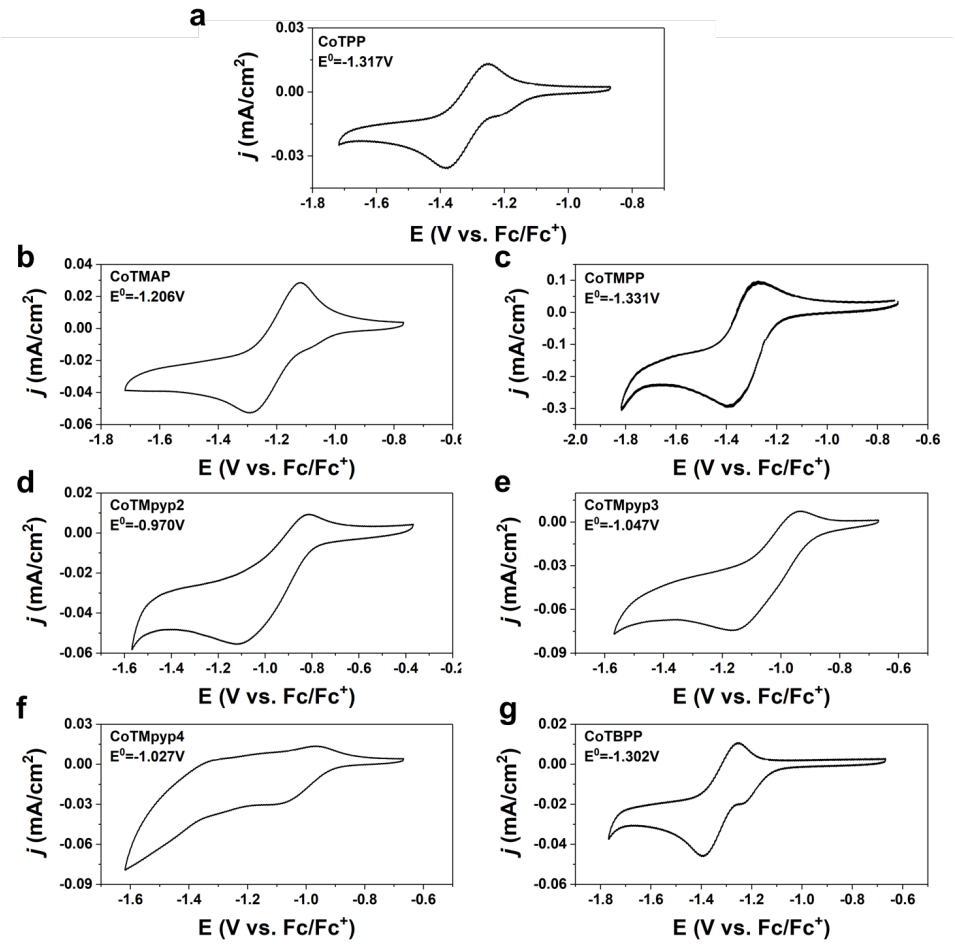

Figure S19. Cyclic voltammograms recorded at a sweep rate of 0.5 V/s on 1mM (a) CoTPP, (b) CoTMAP, (c) CoTMPP, (d) CoTMpyp2, (e) CoTMpyp3, (f) CoTMpyp4 and (g) CoTBPP. Electrolyte solution is 0.1M $TBABF_4$ in DMF/ethanol mixture (vol.% 70:30). A LF-2 reference electrode is calibrated using ferrocene added to the electrolyte.

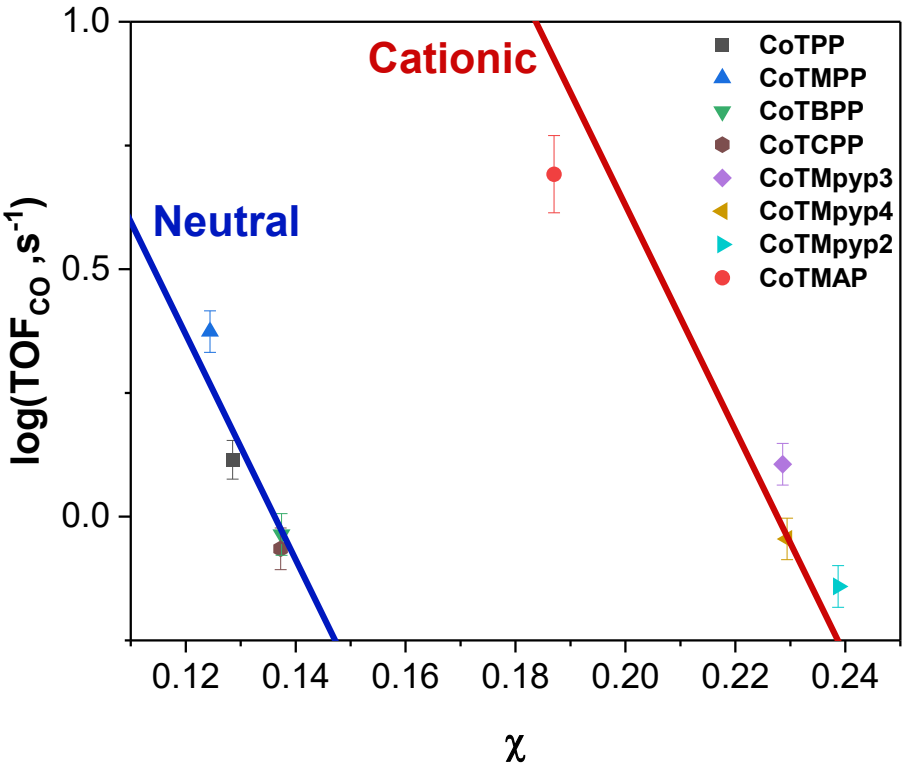

Figure S20. TOF_{CO} of cobalt porphyrin derivatives with various functionalities versus their electronegativity (potential: -0.6 V *vs.* RHE, loading: 8×10^{-10} mol/cm^2).

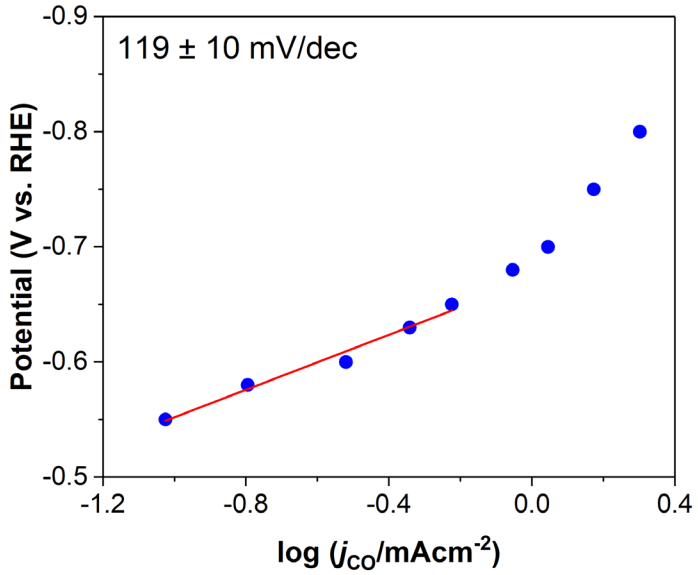

Figure S21. Tafel plot for CoTPP (loading: 8×10^{-10} mol/cm^2). Electrolyte solution is 0.5 M $NaHCO_3$.

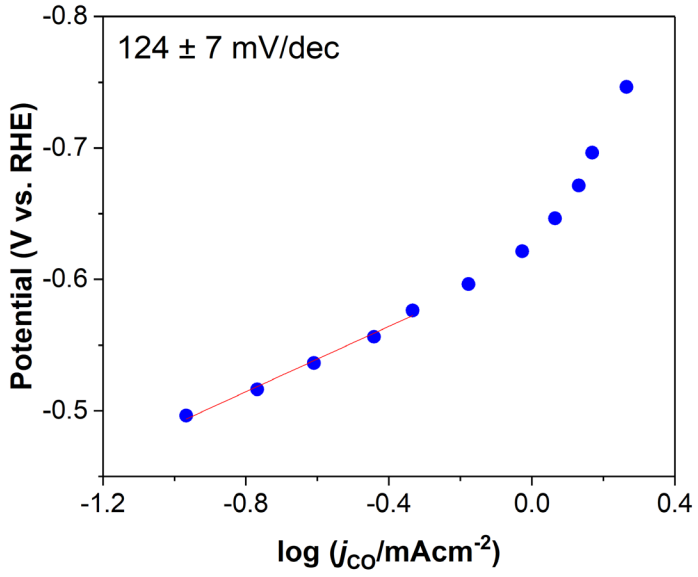

Figure S22. Tafel plot for CoTMAP (loading: 8×10^{-10} mol/cm^2). Electrolyte solution is 0.5 M $NaHCO_3$.

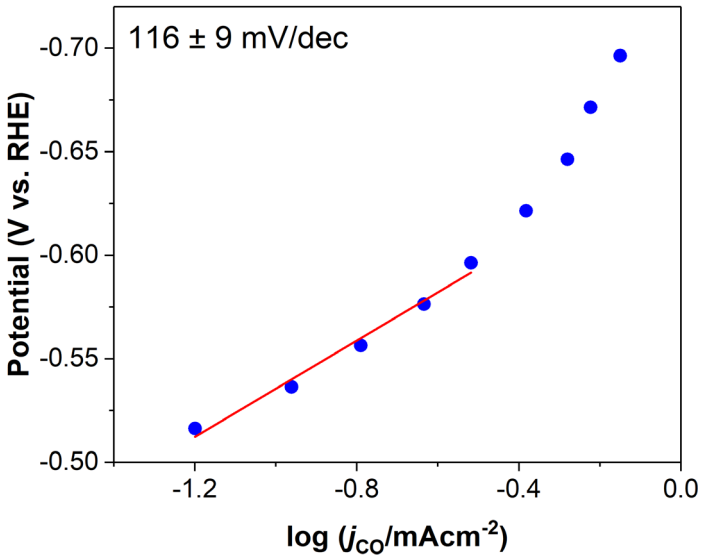

Figure S23. Tafel plot for CoTMPP (loading: 8×10^{-10} mol/cm^2). Electrolyte solution is 0.5 M $NaHCO_3$.

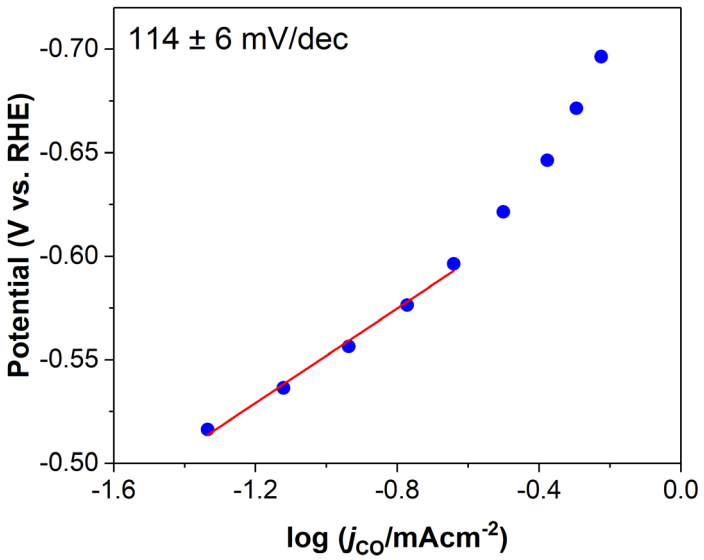

Figure S24. Tafel plot for CoTCPP (loading: 8×10^{-10} mol/cm^2). Electrolyte solution is 0.5 M $NaHCO_3$.

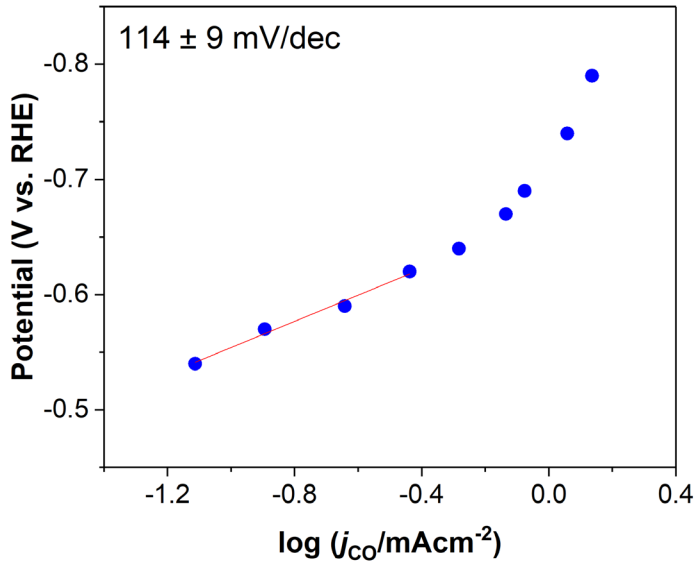

Figure S25. Tafel plot for CoTBPP (loading: 8×10^{-10} mol/cm^2). Electrolyte solution is 0.5 M $NaHCO_3$.

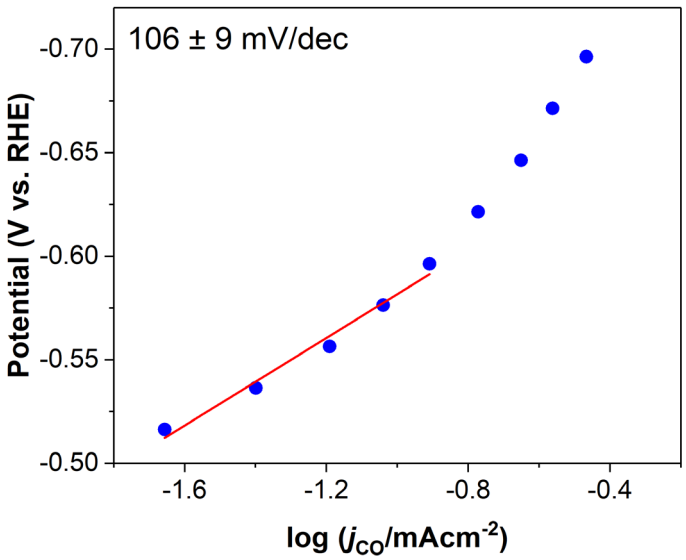

Figure S26. Tafel plot for CoTMpyp2 (loading: 8×10^{-10} mol/cm^2). Electrolyte solution is 0.5 M $NaHCO_3$.

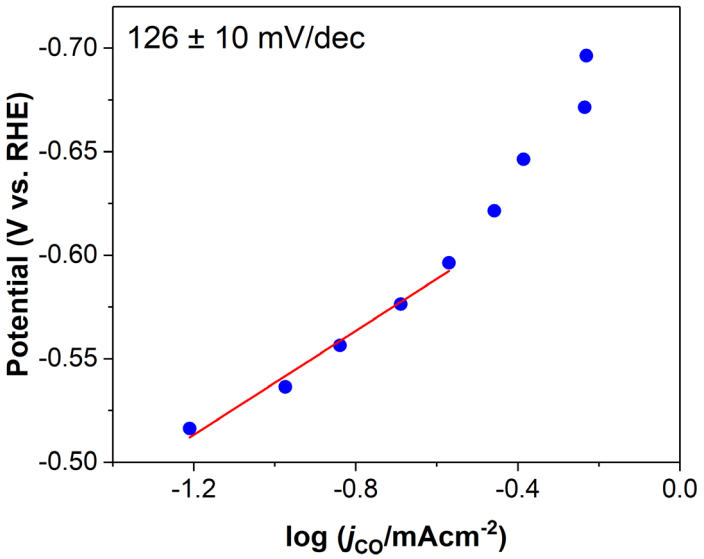

Figure S27. Tafel plot for CoTMpyp3 (loading: 8×10^{-10} mol/cm^2). Electrolyte solution is 0.5 M $NaHCO_3$.

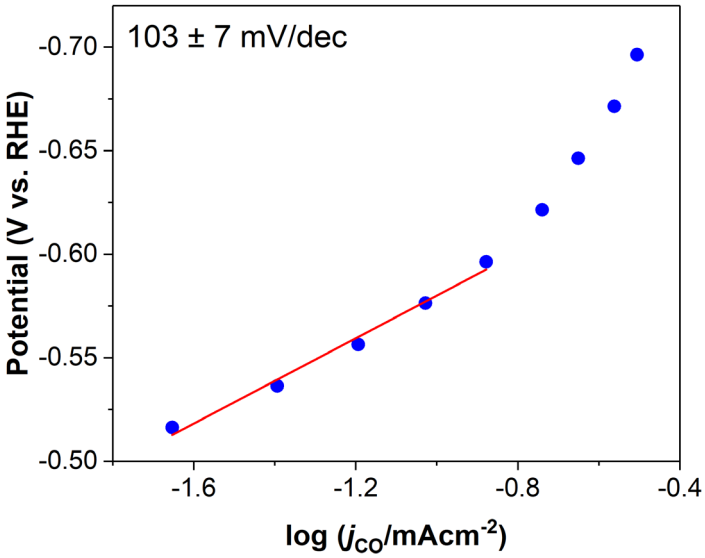

Figure S28. Tafel plot for CoTMpyp4 (loading: 8×10^{-10} mol/cm^2). Electrolyte solution is 0.5 M $NaHCO_3$.

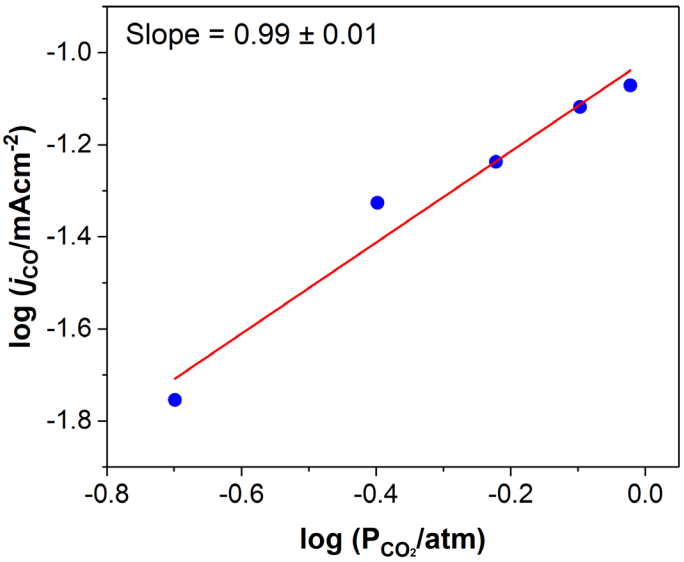

Figure S29. CO partial current density (j_{CO}) as a function of CO_2 partial pressure for CoTPP (loading: 8×10^{-10} mol/cm^2) at -1.3 V *vs.* Ag/AgCl. Electrolyte solution is 0.5 M $NaHCO_3$.

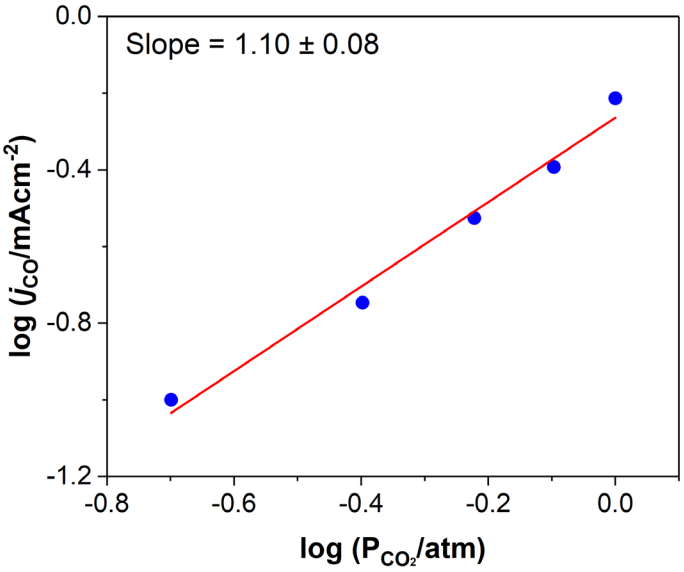

Figure S30. CO partial current density (j_{CO}) as a function of CO_2 partial pressure for CoTMAP (loading: 8×10^{-10} mol/cm^2) at -1.3 V *vs.* Ag/AgCl. Electrolyte solution is 0.5 M $NaHCO_3$.

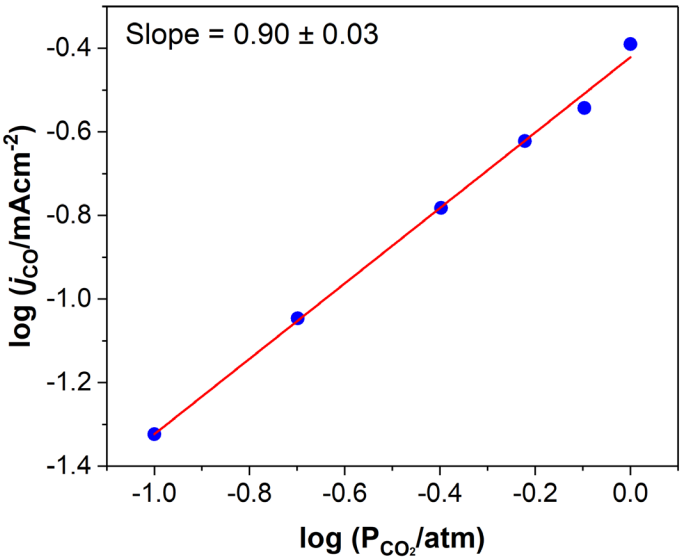

Figure S31. CO partial current density (j_{CO}) as a function of CO_2 partial pressure for CoTMPP (loading: 8×10^{-10} mol/cm^2) at -1.3 V *vs.* Ag/AgCl. Electrolyte solution is 0.5 M $NaHCO_3$.

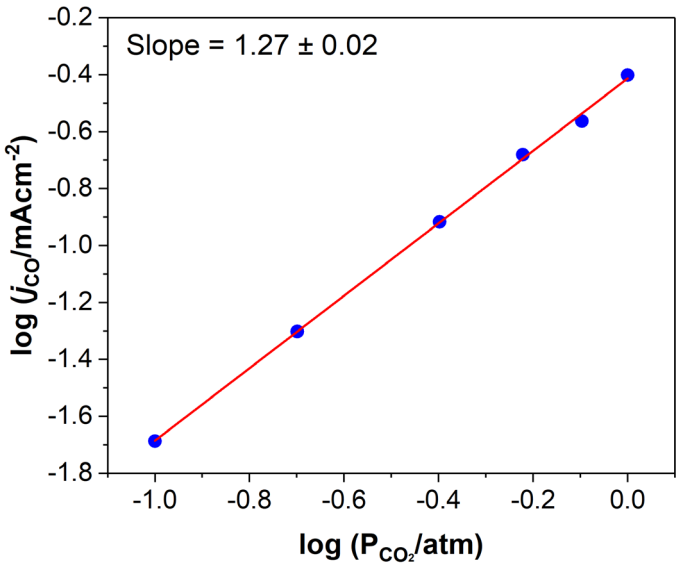

Figure S32. CO partial current density (j_{CO}) as a function of CO_2 partial pressure for CoTCPP (loading: 8×10^{-10} mol/cm^2) at -1.3 V *vs.* Ag/AgCl. Electrolyte solution is 0.5 M $NaHCO_3$.

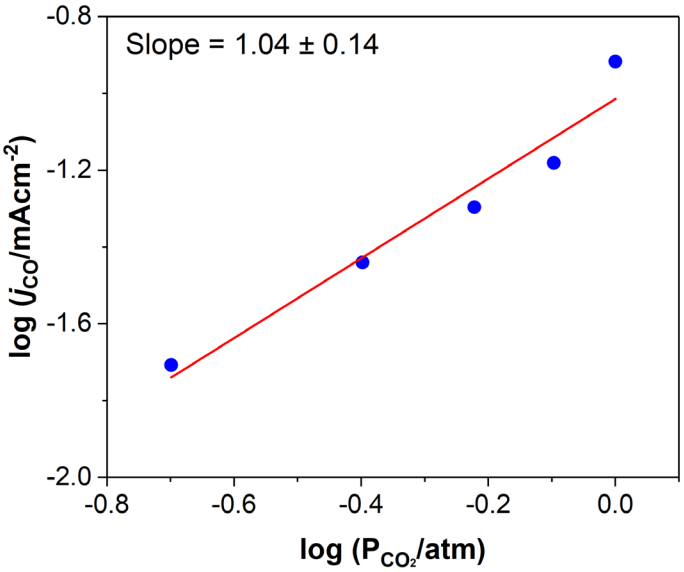

Figure S33. CO partial current density (j_{CO}) as a function of CO_2 partial pressure for CoTBPP (loading: 8×10^{-10} mol/cm^2) at -1.3 V *vs.* Ag/AgCl. Electrolyte solution is 0.5 M $NaHCO_3$.

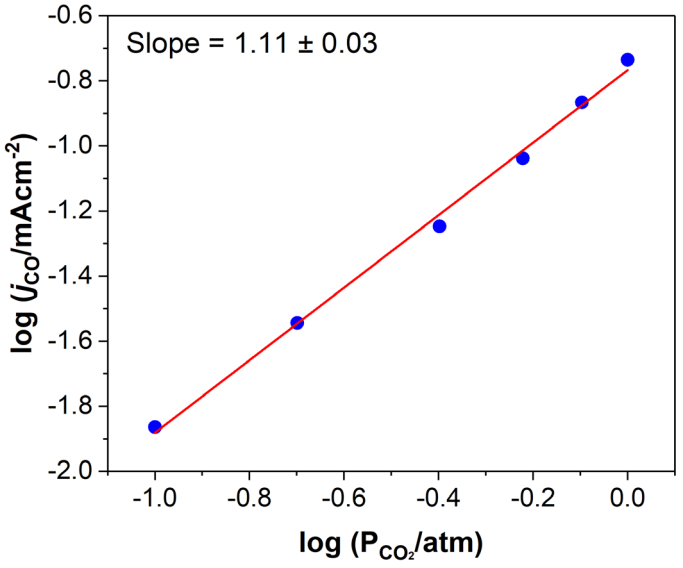

Figure S34. CO partial current density (j_{CO}) as a function of CO_2 partial pressure for CoTMpyp2 (loading: 8×10^{-10} mol/cm^2) at -1.3 V *vs.* Ag/AgCl. Electrolyte solution is 0.5 M $NaHCO_3$.

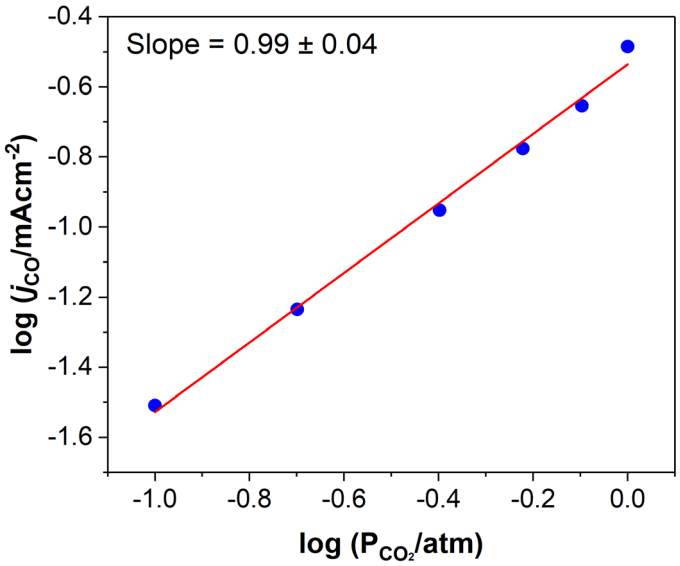

Figure S35. CO partial current density (j_{CO}) as a function of CO_2 partial pressure for CoTMpyp3 (loading: 8×10^{-10} mol/cm^2) at -1.3 V *vs.* Ag/AgCl. Electrolyte solution is 0.5 M $NaHCO_3$.

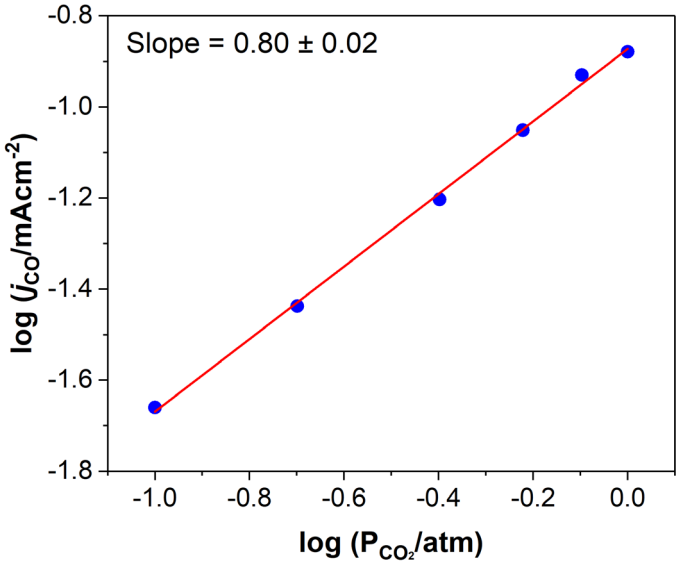

Figure S36. CO partial current density (j_{CO}) as a function of CO_2 partial pressure for CoTMpyp4 (loading: 8×10^{-10} mol/cm^2) at -1.3 V *vs.* Ag/AgCl. Electrolyte solution is 0.5 M $NaHCO_3$.

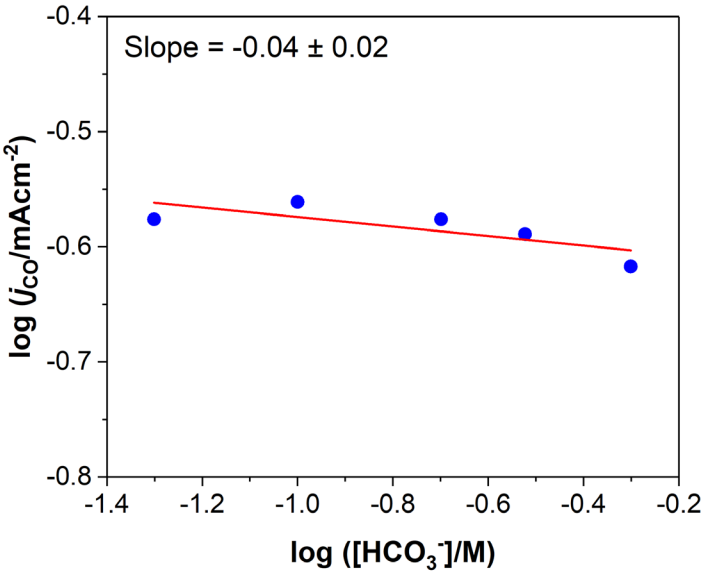

Figure S37. CO partial current density (j_{CO}) as a function of bicarbonate concentration for CoTPP (loading: 8×10^{-10} mol/cm^2) at -1.3 V *vs.* Ag/AgCl.

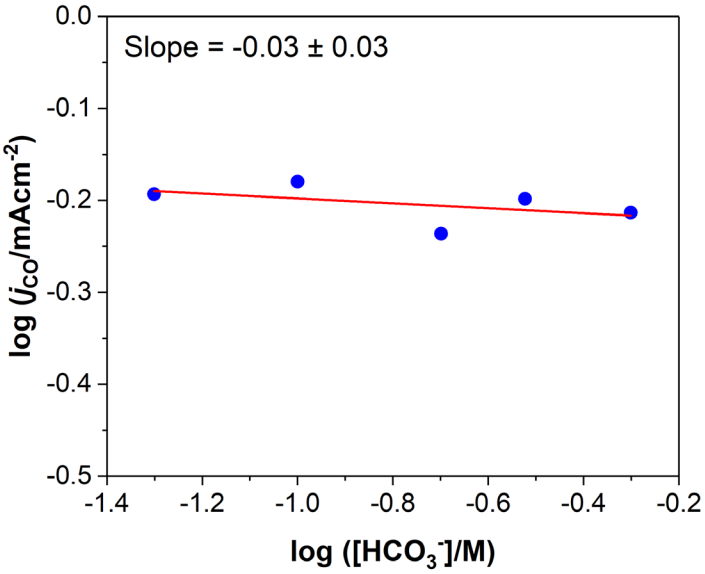

Figure S38. CO partial current density (j_{CO}) as a function of bicarbonate concentration for CoTMAP (loading: 8×10^{-10} mol/cm^2) at -1.3 V *vs.* Ag/AgCl.

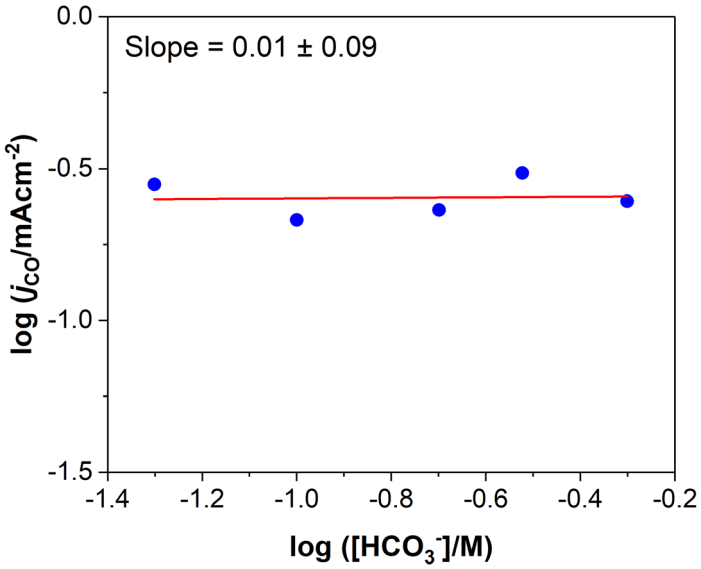

Figure S39. CO partial current density (j_{CO}) as a function of bicarbonate concentration for CoTMPP (loading: 8×10^{-10} mol/cm^2) at -1.3 V *vs.* Ag/AgCl.

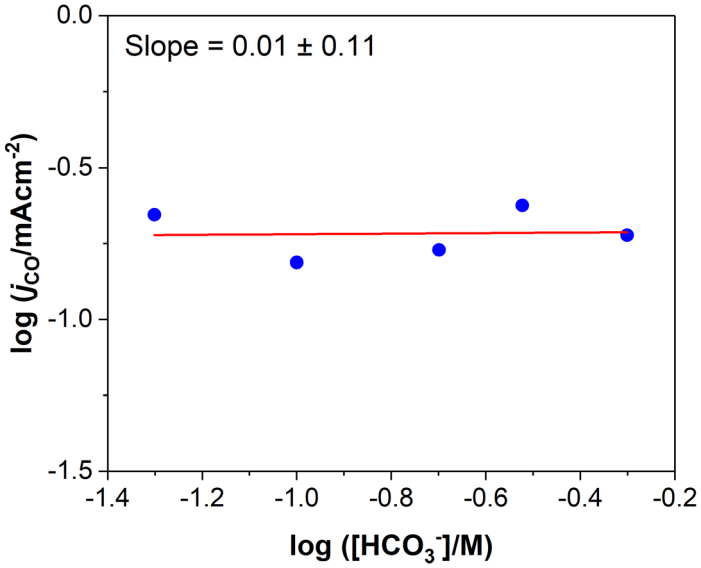

Figure S40. CO partial current density (j_{CO}) as a function of bicarbonate concentration for CoTCPP (loading: 8×10^{-10} mol/cm^2) at -1.3 V *vs.* Ag/AgCl.

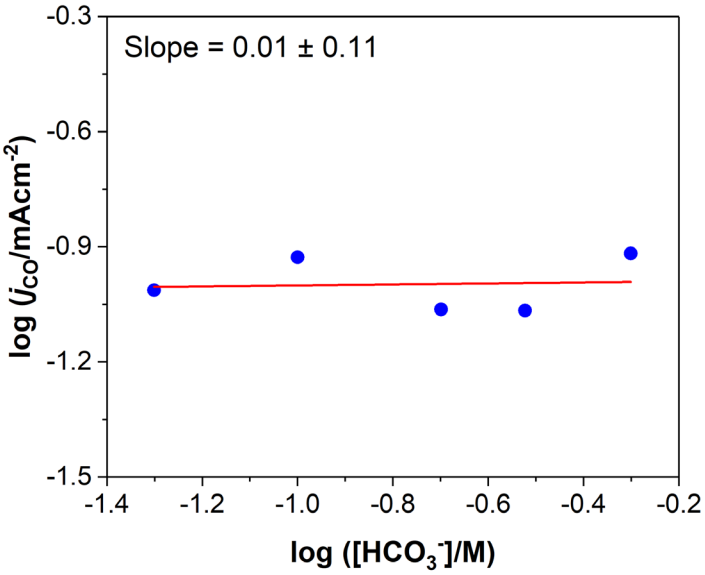

Figure S41. CO partial current density (j_{CO}) as a function of bicarbonate concentration for CoTBPP (loading: 8×10^{-10} mol/cm^2) at -1.3 V *vs.* Ag/AgCl.

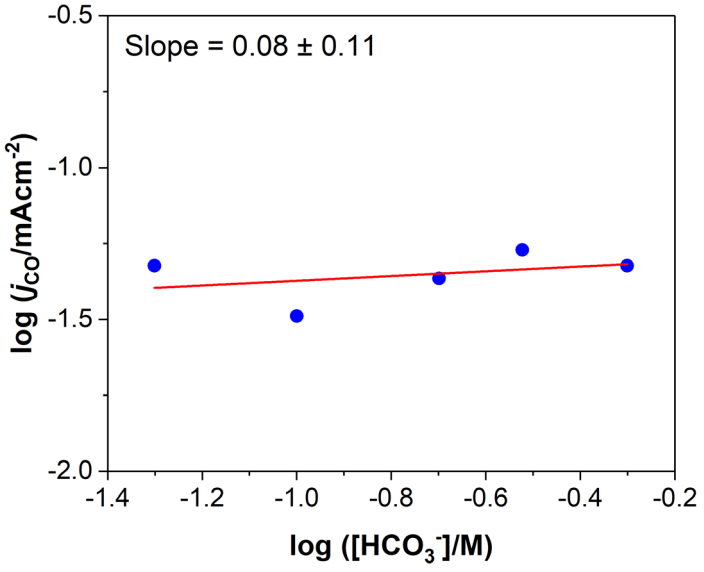

Figure S42. CO partial current density (j_{CO}) as a function of bicarbonate concentration for CoTMpyp2 (loading: 8×10^{-10} mol/m^2) at -1.3 V *vs.* Ag/AgCl.

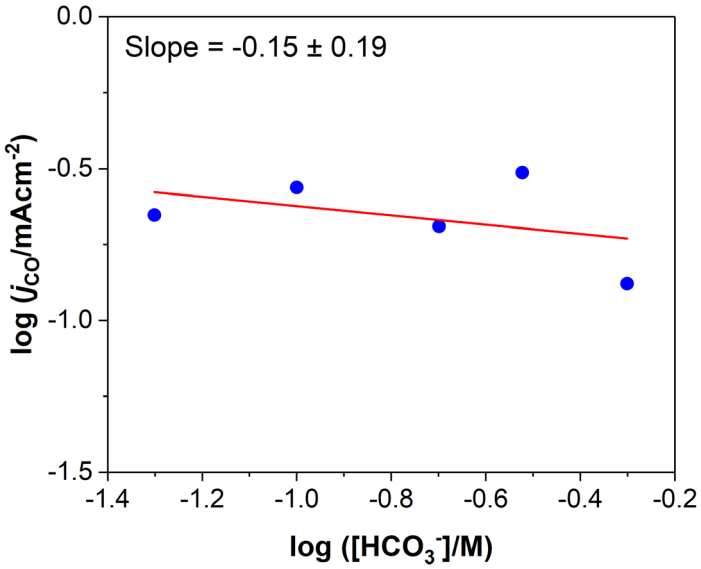

Figure S43. CO partial current density (j_{CO}) as a function of bicarbonate concentration for CoTMpyp3 (loading: 8×10^{-10} mol/cm^2) at -1.3 V *vs.* Ag/AgCl.

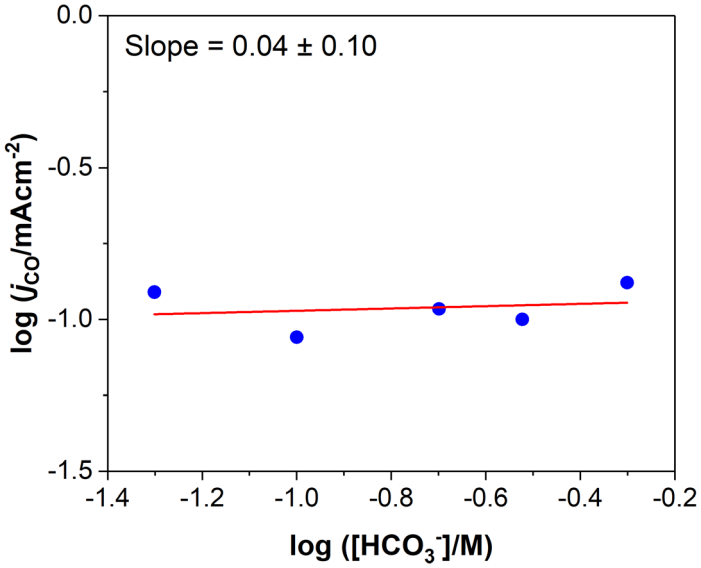

Figure S44. CO partial current density (j_{CO}) as a function of bicarbonate concentration for CoTMpyp4 (loading: 8×10^{-10} mol/cm^2) at -1.3 V *vs.* Ag/AgCl.

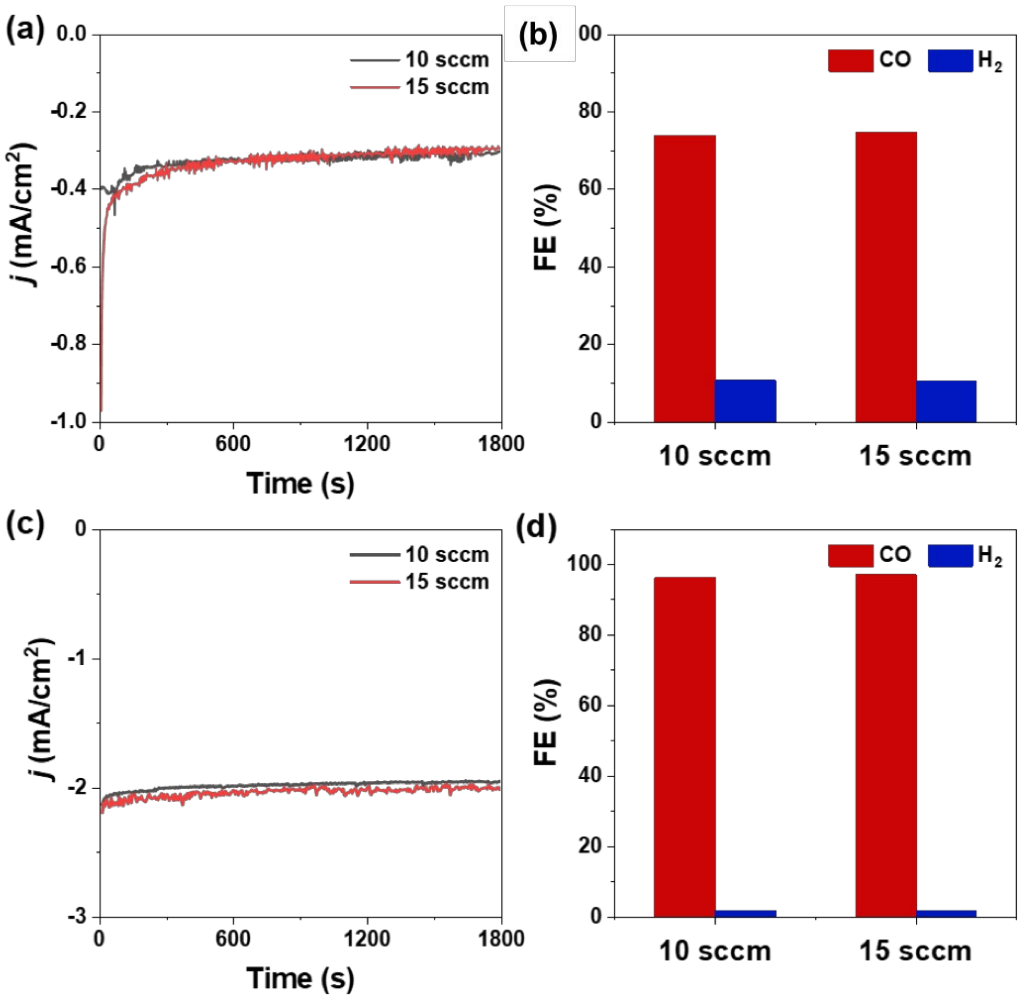

Figure S45. Current densities (a) and Faradaic efficiencies (b) for CoTPP under 10 sccm and 15 sccm CO_2 (potential: -0.6 V vs. RHE, loading: 8×10^{-10} mol/cm^2). (c) and Faradaic efficiencies (d) for CoTPP under 10 sccm and 15 sccm CO_2 (potential: -0.6 V vs. RHE, loading: 4×10^{-8} mol/cm^2).

Table S2. Detailed current densities and Faradaic efficiencies for CoTPP (loading: $1x10^{-8}$ mol/cm^2) at various potentials in 0.5M $NaHCO_3$ electrolyte.

Potential (V vs. RHE)	j (mA/cm^2)	FE_{CO} (%)	FE_{H2} (%)
-0.5	0.55	84.2	10.9
-0.55	1.00	88.7	9.4
-0.6	1.76	96.0	2.7
-0.65	2.46	93.6	3.7

Table S3. Detailed current densities and Faradaic efficiencies for carbon black deposited on carbon paper at -0.6 V *vs.* RHE in 0.5M $NaHCO_3$ electrolyte. The Faradaic efficiency for H_2 at such a low current density is less reliable due to the poor sensitivity of the TCD for small concentrations of H_2, which may contribute to lack of closure.

Catalyst	j (mA/cm^2)	FE_{CO} (%)	FE_{H2} (%)
Carbon Black	0.05	14.3	53.7

Table S4. Detailed current densities, Faradaic efficiencies, and TOF_{CO} for cobalt porphyrins at -0.6 V *vs.* RHE in 0.5M $NaHCO_3$ electrolyte (loading: 8×10^{-10} mol/cm^2). The Faradaic efficiency for H_2 at such a low current density is less reliable due to the poor sensitivity of the TCD for small concentrations of H_2.

Catalyst	***j* (mA/cm^2)**	**FE_{CO} (%)**	**FE_{H2} (%)**	**TOF_{CO}(s^{-1})**
CoTPP	0.30	72.2	16.6	1.31
CoTMPP	0.46	94.1	4.5	2.47
CoTBPP	0.24	72.0	11.6	0.93
CoTCPP	0.22	71.9	10.0	0.87
CoTMAP	0.92	97.8	2.7	5.00
CoTMpyp2	0.26	53.1	29.6	0.73
CoTMpyp3	0.29	78.9	15.7	1.29
CoTMpyp4	0.22	66.0	27.2	0.91
CoTSPP	0.38	76.8	24.2	1.77

Table S5. A comparison of reported porphyrin-based catalysts for the electroreduction of CO_2 to CO in aqueous media to this study. NR indicates that the value is not reported.

Catalyst	*j* (mA/cm^2)	V *vs.* RHE	Electrolyte (pH)	FE_{CO}(%)	TOF_{CO}(s^{-1})	Ref.
CoTPP	0.3	-0.60	0.5M $NaHCO_3$	72.2	1.31	This Study
CoTMAP	0.92	-0.60	0.5M $NaHCO_3$	97.8	5.00	This Study
CoTPP/CNT	NR	-0.70	0.5M $KHCO_3$	~70	2.75	[16]
Fe-CB	~0.5	-0.63	0.5M $KHCO_3$	100	1.74	[17]
Fe-TPP	~0.2	-0.63	0.5M $KHCO_3$	96	0.94	[17]
FeTPP-WSCAT	~1	-0.52	0.1M KCl+0.5M KHCO3	~92	~0.009	[18]
$Al_2(OH)_2$TCPP-Co	~1	-0.67	0.5M $KHCO_3$	76	0.06	[19]
COF-367-Co	3.3	-0.67	0.5M $KHCO_3$	91	0.53	[20]
COF-367-Co(1%)	0.45	-0.67	0.5M $KHCO_3$	53	2.6	[20]
COF-366-(OMe)2-Co	NR	-0.67	0.5M $KHCO_3$	85	0.014	[21]
COF-366-F-Co	NR	-0.67	0.5M $KHCO_3$	96	0.02	[21]

A more comprehensive listing of the activity of all molecular complexes tested under aqueous conditions can be found in Table S3 of Zhu et al.[22] In this listing, the only complexes which exhibit higher activities than the porphyrins are the phthalocyanines.

6. DFT coordinates of optimized structures

Ph (Optimized structure for benzene)

C	0.00000000	0.00000000	0.00000000
C	0.00000000	0.00000000	1.39660354
C	1.20919717	0.00000000	2.09495765
C	2.41871994	0.00024904	1.39671677
C	2.41871821	0.00036503	0.00031759
C	1.20935329	0.00012402	-0.69814144
H	-0.94115438	-0.00016675	-0.54326160
H	-0.94123662	-0.00013477	1.93976631
H	1.20920832	-0.00014802	3.18164493
H	3.35973117	0.00034376	1.94021173
H	3.35982351	0.00046679	-0.54305960
H	1.20960895	0.00016707	-1.78483645

PhBr (Optimized structure for bromobenzene)

C	-2.18102600	1.20778600	-0.00000200
C	-2.88120500	0.00000600	0.00000700
C	-2.18105900	-1.20776800	-0.00001500
C	-0.78491400	-1.21590800	0.00001000
C	-0.10388700	-0.00002000	0.00002300
C	-0.78490500	1.21590300	-0.00000200
H	-2.71864100	2.15208700	-0.00000900
H	-3.96740200	0.00003300	0.00000000
H	-2.71865500	-2.15207900	-0.00002400
H	-0.23311700	-2.14976400	0.00000200
H	-0.23305600	2.14972700	-0.00001300
Br	1.81065300	0.00000000	-0.00000200

PhCl (Optimized structure for chlorobenzene)

C	-1.57458300	-1.20749400	0.00000400
C	-2.27503900	-0.00000200	0.00001000
C	-1.57459700	1.20748600	0.00000000
C	-0.17852800	1.21599900	0.00000500
C	0.50369500	0.00000800	0.00000800
C	-0.17852600	-1.21599800	0.00000100
H	-2.11259600	-2.15145900	0.00000200
H	-3.36125100	-0.00001400	0.00001200
H	-2.11260100	2.15145600	-0.00000300
H	0.37411700	2.14957400	0.00000100
H	0.37414300	-2.14955800	-0.00000400
Cl	2.26492000	0.00000000	-0.00001000

PhOMe (Optimized structure for methoxybenzene)

C	-0.03273100	1.06347800	0.00009800
C	1.33622000	1.35167200	0.00002500
C	2.28355500	0.33084300	-0.00007200
C	1.85194300	-1.00042500	-0.00005900
C	0.49531800	-1.30360700	0.00000000
C	-0.45471000	-0.27116300	0.00004700
H	-0.75045700	1.87606000	0.00022400
H	1.65558800	2.39079700	0.00006100
H	3.34414800	0.56484400	-0.00012300
H	2.57845000	-1.80893700	-0.00011500
H	0.14286100	-2.33049300	-0.00000200
O	-1.76149000	-0.67218100	0.00021100
C	-2.76894300	0.32510600	-0.00018300
H	-3.72054000	-0.20991100	-0.00035900
H	-2.71125900	0.95996300	0.89423300

H	-2.71078000	0.95970600	-0.89474200

PyMe (Optimized structure for methyl pyridinium)

C	0.19142800	-1.17803700	-0.00973900
C	-1.19271500	-1.20487800	0.00278900
C	-1.89942500	-0.00019300	0.00856700
C	-1.19307500	1.20466000	0.00278900
C	0.19111400	1.17824200	-0.00973800
H	0.79734100	-2.07633500	-0.01474100
H	-1.70202000	-2.16198800	0.00463700
H	-2.98480400	-0.00034200	0.01604000
H	-1.70265600	2.16162300	0.00464600
H	0.79669300	2.07674700	-0.01472200
C	2.34590000	0.00001100	0.01516600
H	2.71312700	0.89244800	-0.49144800
H	2.68312900	-0.00626500	1.05453300
H	2.71309600	-0.88620800	-0.50235900
N	0.86096100	0.00021300	-0.01651300

PhNMe3 (Optimized structure for phenyl trimethylammonium)

C	2.17367300	-1.20361200	-0.00000300
C	2.88757700	-0.00396600	-0.00000900
C	2.20054000	1.20741200	0.00000000
C	0.80252800	1.23390400	-0.00001300
C	0.10267600	0.02848200	-0.00005100
C	0.78000900	-1.19427300	-0.00001600
H	2.69718400	-2.15429400	0.00002000
H	3.97277100	-0.01561700	0.00001200
H	2.74411100	2.14677400	0.00002800
H	0.30429400	2.19427900	0.00002300

H	0.25200100	-2.14201700	0.00000600
C	-1.91149400	-0.71505300	-1.23953800
C	-1.91138400	-0.71549000	1.23931800
C	-2.02301900	1.38374600	0.00027000
H	-1.53317900	-0.18830400	-2.11593900
H	-1.54450200	-1.73954800	-1.23644700
H	-3.00284800	-0.70983900	-1.22979200
H	-1.53301300	-0.18903800	2.11587400
H	-3.00273900	-0.71029600	1.22965200
H	-1.54437000	-1.73997800	1.23583800
H	-3.10702900	1.26801100	0.00054500
H	-1.70864800	1.91729700	0.89668700
H	-1.70913500	1.91744300	-0.89622900
N	-1.41307600	0.00260300	-0.00000400

$PhSO_3$ (Optimized structure for benzenesulfonate)

C	-2.36646500	1.20769100	0.00272800
C	-0.97055600	1.20733700	-0.02418300
C	-0.26711400	0.00000600	-0.03190100
C	-0.97055100	-1.20733100	-0.02418400
C	-2.36645800	-1.20769200	0.00272800
C	-3.06980200	-0.00000200	0.01961000
H	-2.90890400	2.15199400	0.00490200
H	-0.40620400	2.13428300	-0.05844600
H	-0.40619800	-2.13427700	-0.05845200
H	-2.90889300	-2.15199800	0.00490100
H	-4.15828100	-0.00000500	0.03793100
S	1.55818400	0.00000100	0.00425700
O	1.92783200	-1.25363300	-0.70720300
O	1.88472700	-0.00014300	1.45569700

O	1.92784400	1.25376800	-0.70696200

7. References

(1) Yoshimoto, S.; Sawaguchi, T. Electrostatically Controlled Nanostructure of Cationic Porphyrin Diacid on Sulfate/Bisulfate Adlayer at Electrochemical Interface. *J. Am. Chem. Soc.* **2008**, *130* (47), 15944–15949.

(2) Lee, C.; Yang, W.; Parr, R. G. Development of the Colle-Salvetti Correlation-Energy Formula into a Functional of the Electron Density. *Phys. Rev. B* **1988**, *37* (2), 785–789.

(3) Becke, A. D. A New Mixing of Hartree–Fock and Local Density-functional Theories. *J. Chem. Phys.* **1993**, *98* (2), 1372–1377.

(4) Becke, A. D. Density-Functional Exchange-Energy Approximation with Correct Asymptotic Behavior. *Phys. Rev. A* **1988**, *38* (6), 3098–3100.

(5) McLean, A. D.; Chandler, G. S. Contracted Gaussian Basis Sets for Molecular Calculations. I. Second Row Atoms, Z =11–18. *J. Chem. Phys.* **1980**, *72* (10), 5639–5648.

(6) Ditchfield, R.; Hehre, W. J.; Pople, J. A. Self-Consistent Molecular-Orbital Methods. IX. An Extended Gaussian-Type Basis for Molecular-Orbital Studies of Organic Molecules. *J. Chem. Phys.* **1971**, *54* (2), 724–728.

(7) Insert Gaussian Citation.

(8) Csizmadia, I. G. *Theory and Practice of MO Calculations on Organic Molecules*; Elsevier, Amsterdam, 1976.

(9) Mulliken, R. S. Electronic Population Analysis on LCAO–MO Molecular Wave Functions. I. *J. Chem. Phys.* **1955**, *23* (10), 1833–1840.

(10) Marriott, S.; Reynolds, W. F.; Taft, R. W.; Topsom, R. D. Substituent Electronegativity Parameters. *J. Org. Chem.* **1984**, *49* (6), 959–965.

(11) Http://Barrett-Group.Mcgill.ca/Tutorials/Gaussian%20tutorial.Pdf.

(12) Www.Huntresearchgroup.Org.Uk/Teaching/Teaching_comp_chem_year4/L7_bonding.Pdf.

(13) Jensen, F. *Introduction to Computational Chemistry*, 1st ed.; Wiley, 1999.

(14) Janata, J. Physical Electrochemistry. Fundamentals, Techniques and Applications. By Eliezer Gileadi. *Angew. Chemie Int. Ed.* **2011**, *50* (41), 9538–9538.

(15) Wuttig, A.; Yoon, Y.; Ryu, J.; Surendranath, Y. Bicarbonate Is Not a General Acid in Au-

Catalyzed CO2 Electroreduction. *J. Am. Chem. Soc.* **2017**, *139* (47), 17109–17113.

(16) Hu, X.-M.; Rønne, M. H.; Pedersen, S. U.; Skrydstrup, T.; Daasbjerg, K. Enhanced Catalytic Activity of Cobalt Porphyrin in CO2 Electroreduction upon Immobilization on Carbon Materials. *Angew. Chemie Int. Ed.* **2017**, *56* (23), 6468–6472.

(17) Smith, P. T.; Benke, B. P.; Cao, Z.; Kim, Y.; Nichols, E. M.; Kim, K.; Chang, C. J. Iron Porphyrins Embedded into a Supramolecular Porous Organic Cage for Electrochemical CO2 Reduction in Water. *Angew. Chemie - Int. Ed.* **2018**, *57* (31), 9684–9688.

(18) Tatin, A.; Comminges, C.; Kokoh, B.; Costentin, C.; Robert, M.; Savéant, J.-M. Efficient Electrolyzer for CO2 Splitting in Neutral Water Using Earth-Abundant Materials. *Proc. Natl. Acad. Sci.* **2016**, *113* (20), 5526–5529.

(19) Kornienko, N.; Zhao, Y.; Kley, C. S.; Zhu, C.; Kim, D.; Lin, S.; Chang, C. J.; Yaghi, O. M.; Yang, P. Metal–Organic Frameworks for Electrocatalytic Reduction of Carbon Dioxide. *J. Am. Chem. Soc.* **2015**, *137* (44), 14129–14135.

(20) Lin, S.; Diercks, C. S.; Zhang, Y.-B.; Kornienko, N.; Nichols, E. M.; Zhao, Y.; Paris, A. R.; Kim, D.; Yang, P.; Yaghi, O. M.; et al. Covalent Organic Frameworks Comprising Cobalt Porphyrins for Catalytic CO2 Reduction in Water. *Science (80-.).* **2015**, *349* (6253), 1208–1213.

(21) Diercks, C. S.; Lin, S.; Kornienko, N.; Kapustin, E. A.; Nichols, E. M.; Zhu, C.; Zhao, Y.; Chang, C. J.; Yaghi, O. M. Reticular Electronic Tuning of Porphyrin Active Sites in Covalent Organic Frameworks for Electrocatalytic Carbon Dioxide Reduction. *J. Am. Chem. Soc.* **2018**, *140* (3), 1116–1122.

(22) Zhu, M.; Ye, R.; Jin, K.; Lazouski, N.; Manthiram, K. Elucidating the Reactivity and Mechanism of CO2 Electroreduction at Highly Dispersed Cobalt Phthalocyanine. *ACS Energy Lett.* **2018**, *3*, 1381–1386.